A lab in the field: High-frequency analysis of water quality and stable isotopes in streamwater and precipitation

Jana von Freyberg[1,2], Bjørn Studer[1], James W. Kirchner[1,2]

[1] Department of Environmental Systems Science, ETH Zurich, Zurich, Switzerland

[2] Swiss Federal Research Institute WSL, Birmensdorf, Switzerland

Correspondence to: Jana von Freyberg (jana.vonfreyberg@usys.ethz.ch)

Abstract. High-frequency measurements of solutes and isotopes (^{18}O and ^{2}H) in rainfall and streamflow can shed important light on catchment flow pathways and travel times, but the workload and sample storage artifacts involved in collecting, transporting, and analyzing thousands of bottled samples severely constrain catchment studies where conventional sampling methods are employed. However, recent developments towards more compact and robust analyzers have now made it possible to measure chemistry and water isotopes in the field at sub-hourly frequencies over extended periods. Here we present laboratory and field tests of a membrane-vaporization continuous water sampler coupled to a cavity ring-down spectrometer for real-time measurements of $\delta^{18}O$ and $\delta^{2}H$, combined with a dual-channel ion chromatograph (IC) for synchronous analysis of major cations and anions. The precision of the isotope analyzer was typically better than 0.03 ‰ for $\delta^{18}O$ and 0.17 ‰ for $\delta^{2}H$, for 10 min average readings taken at intervals of 30 min. Carryover effects were less than 1.2 % between isotopically contrasting water samples for 30 min sampling intervals, and instrument drift could be corrected through periodic analysis of secondary reference standards. The precision of the ion chromatograph was typically ~0.1-1 ppm or better, with relative standard deviations of ~1% or better for most major ions in streamwater, sufficient to detect subtle biogeochemical signals in catchment runoff. We installed the coupled isotope analyzer / IC system in an uninsulated hut next to a stream of a small catchment and analyzed streamwater and precipitation samples every 30 min over 28 days. These high-frequency measurements facilitated a detailed comparison of event-water fractions via end-member mixing analysis with both chemical and isotope tracers. For two events with relatively dry antecedent moisture conditions, event-water fractions were <21 % based on isotope tracers, but were significantly overestimated (40 % to 82 %) by the chemical tracers. These observations, coupled with the storm-to-storm patterns in precipitation isotope inputs and the associated streamwater isotope response, led to a conceptual hypothesis for runoff generation in the catchment. Under this hypothesis, the pre-event water that is mobilized by precipitation events may, depending on antecedent moisture conditions, be significantly shallower, younger, and less mineralized than the deeper, older water that feeds base flow and thus defines the "pre-event" end-member used in hydrograph separation. This proof-of-concept study illustrates the potential advantages of capturing isotopic and hydrochemical behavior at high frequency over extended periods that span multiple hydrologic events.

1. Introduction

Environmental tracers are widely used in hydrology to investigate recharge processes, subsurface flow mechanisms and streamflow components (Leibundgut and Seibert, 2011). The most common environmental tracers are the naturally occurring stable water isotopes ^{18}O and ^{2}H (Klaus and McDonnell, 2013). Solutes such

37 as dissolved organic compounds, nutrients, and major ions are also widely used, together with stable isotopes, as

38 indicators of flowpaths and biogeochemical reactions (e.g., McGlynn and McDonnell, 2003; Vitvar and

39 Balderer, 1997; Weiler et al., 1999). Environmental tracer studies typically involve manual or automated

40 sample collection, followed by transport, storage, and subsequent laboratory analysis. The time and effort

41 involved in sample handling are often a major constraint limiting the frequency and duration of sampling, and

42 thus the scope of tracer studies. While various automated, in-situ analyzers for certain solutes and nutrients are

43 becoming standard tools in environmental monitoring studies (e.g., Bende-Michl and Hairsine, 2010; Rode et

44 al., 2016b), high-frequency analyses of isotopes and major ions over longer time periods remain challenging.

45

46 To date, isotope studies have maintained high sampling frequencies only during a few storm events (e.g.,

47 Berman et al., 2009; Lyon et al., 2008; Pangle et al., 2013), with the result that only limited ranges of catchment

48 behavior have been explored. Long-term catchment studies capture a wider range of hydrologic events, but

49 generally collect water samples at only weekly or monthly intervals for subsequent laboratory analysis (e.g.,

50 Buso et al., 2000; Darling and Bowes, 2016; Jasechko et al., 2016, Neal et al., 2011), making higher-frequency

51 behaviors unobservable. As pointed out by Kirchner et al. (2004), sampling at intervals much longer than the

52 hydrological response times of a catchment may result in significant losses of information. For instance, sub-

53 daily sampling is required to capture diurnal fluctuations in streamwater hydrochemistry, which reflect

54 evapotranspiration effects or in-stream biological activity (e.g., Aubert and Breuer, 2016; Hayashi et al., 2012).

55 In order to differentiate hydrological and biogeochemical catchment processes related to different water ages

56 and flow pathways, long-term monitoring has to be complemented by additional high-frequency hydrochemical

57 and isotope measurements. So far, only a few long-term studies have sampled streamwater at daily or sub-daily

58 intervals for on-site measurements or subsequent analysis in the laboratory, such as at Plynlimon, Wales (Neal

59 et al., 2012), at the Kervidy-Naizin catchment in western France (Aubert et al., 2013) or at the Selke river in

60 Germany (Rode et al., 2016a). Such studies have yielded fundamental insights into catchment hydrological

61 behaviour, not only at a wide range of temporal scales but also under varying hydro-climatic conditions (e.g.,

62 Benettin et al., 2015; Halliday et al., 2013; Harman, 2015; Kirchner and Neal, 2013; Riml and Worman, 2015).

63

64 The recent development of compact and robust isotope analyzers has fostered initial attempts to continuously

65 measure $\delta^{18}O$ and δ^2H in streamwater or precipitation directly in the field. The only previous field-based

66 isotope monitoring of 4 contiguous weeks was carried out by Berman et al. (2009) with a customized liquid

67 water isotope analyzer based on off-axis integrated cavity output spectroscopy (OA-ICOS; Los Gatos Research,

68 Mountain View, CA, USA), which measured $\delta^{18}O$ and δ^2H in 90 samples per day. As the system was based on

69 repeated injections of samples into a vaporizer, daily maintenance (i.e., injection septa change, filter cleaning)

70 was required to keep it running. An alternative approach uses a semi-permeable membrane to generate water

71 vapor from a continuous sample throughflow, which is then transferred to a wavelength scanned – Cavity Ring-

72 Down Spectrometer (CRDS) (e.g., Herbstritt et al., 2012). Munksgaard et al. (2011) developed such a custom-

73 made diffusion sampler and attached it to a CRDS (Picarro Inc., Santa Clara, CA, USA) that was used to

74 measure $\delta^{18}O$ and δ^2H in precipitation at frequencies of up to 30s over a 15day period (Munksgaard et al.,

75 2012), as well as to monitor the isotopic response at 1 min resolution in streamflow during a storm event

76 (Tweed et al., 2016).

77

78 A similar diffusion sampling system has recently become commercially available (Continuous Water Sampler

79 Module, or CWS; Picarro Inc., Santa Clara, CA, USA), which allows for quasi-continuous measurements of

80 $\delta^{18}O$ and δ^2H in liquid water samples when coupled to a CRDS analyzer. Here we present initial laboratory and

81 field verification experiments with this device, which we have combined with a dual-channel ion chromatograph

82 (IC; Metrohm AG, Herisau, Switzerland) for real-time analysis of major cations and anions. Laboratory

83 experiments quantifying the precision and sample carryover memory effects of this system are presented in

84 Section 3 below. Section 4 illustrates the performance of the system in the field using a 28-day deployment at a

85 small catchment in Switzerland. Section 5 quantifies the fractions of event water that contributed to the flood

86 hydrograph in eight storm events, illustrating one potential application of high-frequency measurements of

87 isotopes and major ions.

88 **2. Methodology**

89 **2.1 Isotope analysis and ion chromatography**

90 For the analysis of the stable water isotopes ^{18}O and ^2H, the Continuous Water Sampler module (CWS; Picarro

91 Inc., Santa Clara, CA, USA) was coupled to a Wavelength Scanned-Cavity Ring-Down Spectrometer (WS-

92 CRDS; model L2130-*i*, Picarro Inc., Santa Clara, CA, USA). In the CWS, the water sample flows at a rate of

93 ~1mL min^{-1} through an expanded polytetrafluouroethylene (ePTFE) membrane tube. This tube is mounted in a

94 stainless steel chamber that is supplied with dry air to facilitate the steady diffusion of a small fraction of the

95 through-flowing water as vapor through the membrane. Through the continuous flow of dry air over the outer

96 surface of the membrane, the vapor is carried directly to the CRDS for isotope analysis. To minimize

97 temperature-induced fractionation effects, the instrument keeps the temperatures of the membrane chamber and

98 the inflowing water constant at (± 1 standard deviation) 45±0.1°C and 15±0.1°C, respectively. A solenoid

99 diaphragm pump situated upstream of the membrane cartridge draws water samples from the sample container

100 and pushes them through the membrane tube at a flow rate of approximately 1 mL min^{-1}. As we show in

101 Section 3.1 below, preliminary tests showed that this pump is not sufficient for our purposes, so we substituted a

102 programmable high-precision dosing unit (800 Dosino, Metrohm AG, Herisau, Switzerland) in its place.

103

104 Isotopic abundances are reported through the δ notation relative to the VSMOW-SLAP standards. For the

105 laboratory experiments, we used the factory calibration of the isotope analysis system, because only relative

106 isotope values are needed for quantifying precision, drift, and carryover, and thus the absolute isotope values are

107 unimportant. For the field experiment, however, we periodically measured two internal isotope standards (Fiji

108 and Evian bottled water), which were calibrated by a Picarro L2130-*i* CRDS at the isotope laboratory of the

109 University of Freiburg (Germany) to primary reference materials (IAEA standards SLAP, VSMOW, GISP;

110 instrument precision 0.16 ‰ ($\delta^{18}O$) and 0.6 ‰ (δ^2H)).

111

112   Major ions in liquid water samples, i.e. Na^+, K^+, NH_4^+, Ca^{2+}, Mg^{2+}, F^-, Cl^-, NO_3^-, SO_4^{2-}, PO_4^{3-}, were analyzed

113   with an ion chromatograph (IC; model 940 Professional IC Vario, Metrohm AG, Herisau, Switzerland) with a

114   two-column configuration (Anions: Metrosep A Supp 5 – 250/4.0, Cations: Metrosep c 6 – 250/4.0).

115   Continuous operation of the instrument was possible due to fully automated eluent generation (941 Eluent

116   Production Module). To generate the full ion chromatograms of both anions and cations, approximately 28 min

117   were required; thus the sampling interval of the combined analysis system was fixed at 30 min.

2.2 Sample collection and distribution

119   The water samples were distributed between the analyzers with high-precision dosing units (800 Dosino, here

120   called simply 'Dosino'; Metrohm, Herisau, Switzerland). A Dosino contains a programmable piston that fills

121   and empties a glass cylinder with up to 50 mL of sample at a resolution of 10,000 increments (implying 5 μL

122    $increment^{-1}$). The design of the dosing unit minimizes the dead volume and thus the potential for sample

123   carryover. In the base of the glass cylinder sits a rotating valve disc that guides the liquid sample through one of

124   four ports; thus each Dosino functions as both a switching valve and a syringe pump.

125

126   Figure 1 depicts the schematic overview of the automatic sample collection and analysis system, showing how

127   the different Dosinos distribute precipitation and streamwater samples between the isotope analyzer, the IC and

128   an autosampler (which can be programmed to save individual samples for subsequent analysis in the

129   laboratory). The sampling routine begins with a cleaning step when either the 'P Dosino' (which handles

130   precipitation) or the 'S Dosino' (which handles streamwater) transports 10 mL of sample water for rinsing to a

131   sample storage beaker. The 'Isotope Dosinos' also eject any remaining sample into the beaker, after which the

132   beaker is emptied. Then, 50 mL of fresh streamwater or precipitation sample is transported (by either the 'S

133   Dosino' or the 'P Dosino' for streamwater or precipitation, respectively) into the rinsed beaker, from which one

134   of the 'Isotope Dosinos' draws 30 mL of water and injects it at a flow rate of 1 mL min^{-1} into the CWS for

135   isotope analysis. The two 'Isotope Dosinos' operate alternatingly to minimize the time when the sample flow

136   into the CWS is interrupted. Meanwhile, either the 'P Dosino' or the 'S Dosino' takes up another 12 mL of

137   water sample and pumps it through a 0.45 μm tangential filter into the 'IC Dosino', which discards the first

138   2 mL of the filtered sample. From the remaining filtered sample, 8 mL are filled into vials by the autosampler

139   and 2 mL are delivered to the IC for direct ion analysis. During the ion analysis (ca. 28 min), the 'S Dosino', 'P

140   Dosino' and 'IC Dosino', the autosampler, and all tubing are rinsed with nanopure water to minimize carryover

141   effects. The entire sampling routine is programmed with the IC control software MagIC Net (Metrohm,

142   Herisau, Switzerland), which facilitates detailed data logging and documentation of the sample handling.

3. Laboratory experiments

3.1 Optimization of sample injection into the Continuous Water Sampler module (CWS)

145   In the original design of the CWS, water samples are transported by a small solenoid diaphragm pump between

146   the inlet port and the membrane cartridge at a flow rate of approximately 1 mL min^{-1}. During preliminary tests,

147   however, we observed that raising or lowering the sample container detectably altered the reported isotope

148   ratios. In order to quantify the sensitivity of the instrument to hydraulic head differences (i.e., the height of the

149   water table in the sample bottle relative to the waste outlet of the CWS), we changed the elevations of the

150   sample container relative to the instrument while continuously analyzing a single water sample (nanopure

151   water). We measured the vapor concentration, $\delta^{18}O$ and δ^2H for the same water sample at five different

152   elevations, ranging from 7 cm above to 98 cm below the waste outlet. The end of the waste outlet tube was

153   always freely draining. Each configuration was measured for one hour and the average values and standard

154   deviations of the uncalibrated 6 s measurements of vapor concentration, $\delta^{18}O$ and δ^2H were calculated from the

155   last 10 min of each 1 h configuration.

156

157   The results of this experiment are summarized in Fig. 2, which shows clear linear relationships between the

158   hydraulic head differences and both the vapor concentrations and the isotope measurements. Lowering the

159   sample source relative to the outflow results in systematically heavier isotopic values in the vapor measured by

160   the instrument. Vapor concentrations show a similar trend, i.e. more vapor was generated for lower positions of

161   the sample source. These observations suggest that the hydraulic head difference directly affected the flow rate

162   of the liquid sample through the CWS membrane tube. Because the water is much colder than the surrounding

163   air as it enters the membrane chamber, it is continuously warming as it travels through the membrane tube. At

164   greater head gradients (and thus smaller flow rates), the sample will travel more slowly through the membrane

165   chamber and will warm up more. At higher water temperatures, water should diffuse more rapidly through the

166   membrane and the resulting vapor will be less fractionated relative to the liquid phase (Kendall and McDonnell,

167   1998), as observed in Fig. 2.

168

169   It is unknown whether the empirical linear relationships shown in Fig. 2 are generally applicable, or are specific

170   to each individual membrane or to the properties of the sample. Nevertheless, for this membrane and this

171   sample, the results indicate that changing the hydraulic head by 50 cm changes the reported isotope values by

172   approximately 0.12 ‰ for $\delta^{18}O$ and 0.52 ‰ for δ^2H, respectively. This flow-rate artifact might become

173   particularly important for applications in which isotope standards and samples are drawn from sample

174   containers at different elevations relative to the waste outlet of the CWS (e.g. shipboard sampling). In such

175   cases, a vapor concentration correction relative to a reference height would have to be carried out.

176   Alternatively, a different injection system could be used to deliver a specified flow rate, independent of the

177   position of the source relative to the CWS. We used the Dosino for this purpose, since it functions as a high-

178   precision syringe pump whose delivery rate is specified by the pulse rate of the stepper motor, independent of

179   the hydraulic head gradient.

180

181   Because of the limited volume of each Dosino's glass cylinder (50 mL), a sample could be injected at a flow

182   rate of 1 mL min^{-1} for a maximum of 50 min. For longer injections, or to switch samples, a second Dosino had

183   to take over the sample delivery. The handoff between the Dosinos interrupted the sample flow to the CWS for

184   around 2 s. This interruption was reflected in a sharp but brief increase in vapor concentrations and isotope

185   values, which returned back to stable values approximately 10 min after the injection started (see Fig. 3 for an

186   example). For our application, i.e. synchronous IC measurements, we programmed a 30 min injection period

187   for the isotope analysis. To obtain the final isotope values of a liquid sample we averaged the individual 6 s

188 measurements reported by the WS-CRDS during the last 10 min of each 30 min injection period, using the first
189 20 min to minimize any memory effects from the previous sample or from Dosino changeover. The advantage
190 of the Dosino-based sample handling system is the very steady, pressure-independent sample injection.

191 **3.2 Performance of the isotope analyzer with Continuous Water Sampler (CWS)**

192 We quantified precision, drift coefficients and carryover effects of the isotope analyzer with CWS and Dosino-
193 based sample injection, using a continuous 48-hour laboratory experiment that alternated between three water
194 samples (i.e., to mimic streamwater, precipitation and a reference standard). The sample handling system was
195 as shown in Fig. 1, except that the precipitation collector was replaced with a 10 L bottle of nanopure water and
196 the streamwater sampler was replaced by a 10 L bottle of tap water. The sampling system alternated between
197 these two sources, and for each eighth injection it introduced an isotopically heavier secondary standard (Fiji
198 bottled water) (Fig. 3). The isotopic differences between Fiji bottled water and tap water were about (±standard
199 error, SE) 4.54 ± 0.02 ‰ and 32.67 ± 0.08 ‰ for $\delta^{18}O$ and δ^2H, respectively. The isotopic differences between
200 tap water and nanopure water were much smaller (0.05 ± 0.01 ‰ for $\delta^{18}O$ and 0.12 ± 0.03 ‰ for δ^2H) because
201 the nanopure water was generated from the same tap water by reverse osmosis.

202

203 The precisions of the isotope values, as quantified by the standard deviations of the individual 6s measurements
204 during the last 10 min of each injection period, were better than 0.08 ‰ for $\delta^{18}O$ and 0.18 ‰ for δ^2H. These
205 standard deviations imply that the standard errors of the 10 min averages should be better than 0.008 ‰ and
206 0.018 ‰ for $\delta^{18}O$ and δ^2H, respectively. These standard errors overestimate the repeatability of successive
207 measurements, however. As a measure of sample-to-sample repeatability, the standard deviations of the 10 min
208 averages for the entire 48-hour experiment were 0.03 ‰ ($\delta^{18}O$) and 0.17 ‰ (δ^2H), or better, for each of the three
209 water samples (excluding two outliers associated with an interruption in the sampling routine), much larger than
210 the calculated standard errors. Thus, the major uncertainties in the 10 min averages do not arise from the
211 counting statistics of the instrument itself, but rather, we suspect, from sample-to-sample variability in the
212 performance of the vaporizer. We use these larger estimates of uncertainty (0.03 ‰ for $\delta^{18}O$ and 0.17 ‰ for
213 δ^2H) in the error propagation calculations presented in Section 5.1.

214

215 Instrument drift was analyzed by linear regression of the 10 min averages from the ends of each 30 min
216 injection period. Instrument drift for $\delta^{18}O$ was statistically indistinguishable from zero for two of the three
217 waters, averaging (±SE) -0.009±0.008, -0.009±0.006, and -0.015±0.007 ‰ day^{-1} for Fiji, nanopure, and tap
218 water, respectively. Instrument drift for δ^2H was slow but statistically significant for two of the three waters,
219 averaging 0.133±0.040, 0.084±0.016, and -0.021±0.021 ‰ day^{-1} for Fiji, nanopure, and tap water, respectively.
220 Thus, the accumulated drift over one day was typically smaller than the measurement precision for individual
221 10 min averages for either isotope. As explained in Section 4.2 below, substantially faster drift occurred during
222 the field experiment that could, however, easily be measured and corrected using regularly injected reference
223 standards. This faster drift can be explained with biofilm growth on the membrane, which could be observed on
224 the inside of the membrane tube during preliminary tests with streamwater samples at the field site.

225

226 Between-sample memory mainly arises from small remnants of previously injected samples that remain in the

227 sample handling system (e.g., tubes, membrane, valves, pumps) or the analyzer itself, and are carried over to the

228 following analysis. We quantified the between-sample memory effect of the isotope analyzer using two

229 isotopically contrasting samples, Fiji water and nanopure water. The true isotopic difference was obtained from

230 the 7th (=last) injection of nanopure water, which was measured around 3 h after the reference standard (Fiji),

231 and was thus assumed to be free of any memory effects. We calculated the memory coefficient (X) as a measure

232 of carryover effects using Gupta et al. (2009):

233 $$X = \frac{C_i - C_{i-1}}{C_{true} - C_{i-1}} \qquad\qquad (1)$$

234 where C denotes the isotope ratio (or the solute concentration), the indices (i) and ($i-1$) denote the current and

235 the previous injection, and ($true$) denotes the true value taken from the last value of multiple injections. Based

236 on the 10 min averages from the end of each 30 min injection period, the average carryover from the Fiji bottled

237 water to the next sample was $100\% \cdot (1-X) \approx 0.9$ % for $\delta^{18}O$ and 1.2 % for δ^2H, respectively (Table 1). The

238 carryover during the first and second 10 min of each 30 min injection period was, however, much larger (up to

239 53 % and 6 %, respectively) implying that our 30 min sampling cycle is indeed necessary to prevent

240 unacceptably large carryover effects.

3.3 Performance of the ion chromatograph (IC)

242 With the IC, a 48-hour laboratory experiment was carried out as well. However, the sampling sequence differed

243 slightly from that of the isotope analyzer described previously: each measurement of tap water or Fiji water was

244 followed by two to six samples of nanopure water, which mimics precipitation samples with generally very low

245 solute concentrations. Due to the low solute concentrations in the nanopure water, carryover effects can be

246 quantified efficiently.

247

248 Average concentrations of the major anions and cations during the 48-hour experiment are reported in Table 1,

249 along with their absolute and relative standard deviations. For tap water and Fiji water, relative standard

250 deviations were <5% for all constituents with concentrations above the limit of quantification (LOQ) and ~1%

251 or less for most major ions, indicating that the IC measurements were stable over the 48-hour period and that

252 they were sufficiently precise to detect even subtle biogeochemical signals in streamwater. Drift effects in the

253 instrument were not statistically significant (p>0.05) for most constituents in Fiji water and tap water. For Cl^{-},

254 NO_3^- and SO_4^{2-} in the Fiji water, the linear drift was statistically significant but also very slow: accumulated drift

255 over 24h was never much larger than the LOQ (Table 1). Average % carryover ($100\% \cdot (1-X)$, Eq. (1)) in the

256 nanopure water sample, following immediately after a tap water or Fiji water sample, was ≤ 3.8 %.

4. Application in the field

4.1 Setup

259 For the field experiment, the system was installed in a hut (area 1.7x1.7m) next to a small perennial stream

260 flowing behind the Swiss Federal Institute for Forest, Snow and Landscape Research (WSL) near Zurich,

261 Switzerland. The creek drains an area mainly covered with open grassland, grain fields, and suburban

262 residential neighbourhoods (Fig. 4). The dominant soil type is colluvial, partly gleyic brown soil (GIS-ZH,

263 2016).

265 Stream stage, temperature and electrical conductivity of streamwater were recorded in the stream every 10 min

266 using a data-logging sonde (model DL/N 70; STS SensorTechnik Sirnach, Switzerland). The volumetric

267 discharge was not gauged, but we assume that the times of the highest stream stage coincided with peak flow,

268 and thus use both terms synonymously. Once a day at 7:30 am, daily precipitation was measured with a heated

269 collector and snow depth was recorded. For a higher temporal resolution we used the hourly CombiPrecip

270 dataset (MeteoSwiss), a grid-data product that combines radar estimates and rain-gauge measurements to

271 compute precipitation rates at 1 km^2 spatial resolution. A good agreement ($R^2 = 0.86$) between measured daily

272 precipitation at our field site and the daily sums of hourly CombiPrecip data indicate that the CombiPrecip

273 dataset is a reasonable proxy for precipitation variability at the field site. To distinguish rain and snowfall

274 events, air temperature was recorded near the instrument hut every 10 min (Haeni, 2016; Schaub et al., 2011).

275 The uninsulated hut was not temperature controlled; however, the instruments produced heat so that inside air

276 temperatures were on average 12°C higher than outside. Outside air temperature variations were reflected

277 inside the hut, where air temperatures ranged from 7 to 23°C.

279 A submersible pump (Eheim GmbH, Deizisau, Germany) continuously pumped streamwater at a rate of

280 6 L min^{-1} into a through-flow bucket inside the hut. The volume of the bucket was 10 L; thus every several

281 minutes the contents of the bucket were effectively exchanged. Every 30 min, water was drawn from the bucket

282 by the 'S Dosino' through a 1μm cellulose filter to supply the isotope analyzer, IC and autosampler (Fig. 1).

283 Precipitation was collected with a heated 45 cm diameter funnel installed 2.5 m above ground. Precipitation

284 flowed into a Teflon®-coated collector with a level detector. The status of the level detector was queried before

285 the end of each measurement routine and a precipitation sample was taken only if the threshold volume of

286 72 mL (equaling roughly 0.5 mm of precipitation) was exceeded. For initial filtration of the precipitation

287 sample, a ceramic frit filter was attached on the suction tube of the 'P Dosino' that drew the sample from the

288 precipitation collector. After precipitation was sampled, a peristaltic pump emptied the precipitation collector to

289 avoid mixing fresh and old precipitation samples. The sampling routine was programmed to always alternate

290 between streamwater and precipitation samples in order to obtain enough streamwater samples during storm

291 periods. To reduce biofilm growth on the membrane in the CWS, copper wool was placed in the beaker from

292 which the 'Isotope Dosinos' drew the samples. Sampling was interrupted approximately once a week for basic

293 maintenance (i.e., replacing the filter membranes, cleaning Dosinos, refilling reference standards and eluent

294 stock solutions).

296 To correct for instrument drift, internal reference standards were analyzed every 3h. For the five samples

297 between two bracketing measurements of the same reference standard following equation was applied:

298 $$C_{corr} = C_{raw} + (C_{true} - \frac{C_{std,i} + C_{std,j}}{2}) \hspace{4cm} (2)$$

299 with *C* denoting the solute concentration or the isotope ratio, respectively. The indices represent the corrected

300 value (*corr*), the current raw measurement (*raw*), the true value of the reference standard (*true*), and the

301   previous and successive measurements of the same reference standard (*std*) measured at time *i* and 3h later at

302   time *j*. For the isotope analyzer, Fiji bottled water was used as internal reference standard, which was injected

303   directly from a container by one of the 'Isotope Dosinos' (Fig. 1). The measurements of the IC were drift-

304   corrected with another reference standard (Evian bottled water) that was transferred directly to the IC by the 'IC

305   Dosino'. Evian bottled water was used, as its mineral composition resembles that of streamwater more closely

306   than Fiji bottled water does.

307   **4.2 Temporal high-resolution measurements of stable isotopes and major ions in precipitation and**
308   **streamwater**

309   The measurement system was deployed at the field site from 13 February 2016 to 11 March 2016 and more than

310   1000 streamwater and precipitation samples were analyzed for stable water isotopes and major ions, capturing a

311   wide range of hydrological and hydrochemical conditions. Table 2 provides an overview of the eight storm

312   events during that period. Air temperature measurements at the site and daily observations of the snow height

313   showed that precipitation during Events #1-#7 was mostly rainfall. Snowfall occurred occasionally after 1

314   March, while during Event #8 most precipitation fell as snow.

315

316   We calculated the response time of streamflow as the time difference between the first detection of precipitation

317   and the first significant increase in streamwater level relative to the initial conditions. Response times were

318   between 0 h and 2.5 h (Table 2), suggesting fast runoff from the residential area in the eastern part of the

319   catchment. The most delayed streamflow response (2.5h) was observed after the snowfall Event #8, reflecting

320   delayed snowmelt. As illustrated by Fig. 5, a 30 min sampling interval was sufficient to resolve the temporal

321   patterns of stable isotopes and solutes in streamflow during the rising limb of the hydrograph, even during low-

322   intensity precipitation periods such as Event #5.

323

324   Compared to the laboratory experiment with the isotope analyzer, during the field experiment we observed

325   carryover effects in the isotope measurements of up to $100\% \cdot (1-X)=3\%$, which can be explained by the copper

326   wool in the beaker from which the "Isotope Dosinos" drew the water samples. Despite the rinsing routine of the

327   beaker, the wool retained small volumes of sample from previous injections that affected the isotopic

328   composition in the fresh sample. Consequently, the wool was removed and the prior isotope measurements

329   were adjusted with $X=97\%$ and Eq. (1). Further, instrument drift was substantially faster during the beginning

330   of the field experiment due to biofilm growth in the membrane tube. For instance, during the first week,

331   instrument drift for raw $\delta^{18}O$ and δ^2H measurements in Fiji bottled water was statistically significant, averaging

332   ($\pm SE$) -0.185±0.006 and -0.288±0.015 ‰ day^{-1}, respectively. The variations of air temperature outside and

333   inside the hut were not reflected in the isotope measurements because the CWS regulates inlet air and water

334   temperatures using Peltier thermoelectric controllers.

335

336   Figure 6a illustrates that the isotopic composition of precipitation varied over a range of 15.72 ‰ in $\delta^{18}O$ and

337   115.63 ‰ in δ^2H. By capturing many precipitation events over weeks to months, our isotope analysis system

338   provides a more detailed insight into the variability of precipitation isotopes compared to previous studies that

339   only monitored individual storms at high frequency (e.g., Moerman et al., 2013; Pangle et al., 2013; Tweed et

340   al., 2016). At our site, a correlation between air temperature and the isotopic composition of precipitation is

341   evident for most storm events. Figure 5 shows that, for instance, precipitation samples became isotopically

342   heavier during Events #2 and #8 when air temperature increased, while the precipitation samples became

343   isotopically lighter during Events #1, #3 and #5, when air temperature decreased. During Events #4, #6 and #7,

344   however, the correlation with temperature was not as distinct as during the other five events.

345

346   The isotopic composition of streamwater varied by less than half as much as that of precipitation, i.e. by 6.24 ‰

347   for δ^{18}O and by 45.11 ‰ for δ^2H, respectively (Fig. 6b). For all eight events, the isotopic signature of pre-event

348   streamwater was relatively constant, averaging -11.04±0.21 ‰ for δ^{18}O and -76.97±1.46 ‰ for δ^2H,

349   respectively (±standard deviation, n=8). During the events, δ^{18}O and δ^2H in streamwater changed by up to

350   4.80 ‰ and 36.38 ‰, respectively (Event #7).

351

352   For the IC, memory effects were negligible during the field experiment (because the sample did not make

353   contact with the copper wool), so the measurements were corrected only for drift effects. Solute concentrations

354   in precipitation and streamwater varied widely, as shown for instance in Fig. 5. For Li^+, NH_4^+, K^+, F^- and PO_4^{3-}

355   in streamwater, as well as concentrations of Mg^{2+} in precipitation, measured concentrations were generally

356   below the LOQ. Ca^{2+}, NO_3^- and SO_4^{2-} in streamwater exhibited clear dilution patterns during all precipitation

357   events (Fig. 5e-g). Concentrations of Ca^{2+}, NO_3^- and SO_4^{2-} in precipitation during the eight events were on

358   average (±standard deviation) 12.1±2.9 mg L^{-1}, 1.5±1.1 mg L^{-1} and 0.5±0.8 mg L^{-1}, respectively. Solute

359   concentrations in pre-event streamwater were on the order of (±standard deviation) 160.8±9.7 mg L^{-1} for Ca^{2+},

360   11.7±1.8 mg L^{-1} for NO_3^- and 21.5±3.3 mg L^{-1} for SO_4^{2-}, whereas concentrations during storm events dropped to

361   values as low as 64.6 mg L^{-1} (Ca^{2+}), 3.73 mg L^{-1} (NO_3^-) and 5.12 mg L^{-1} (SO_4^{2-}). In contrast, EC and the

362   concentrations of Cl^- (and Na^+, not shown) in streamwater showed dilution patterns until Event #3, and then

363   showed distinct enrichment patterns thereafter (Fig. 5d), likely associated with road salt wash-off. Due to

364   possible road-salt effects on Na^+ and Cl^-, we will focus on Ca^{2+}, NO_3^- and SO_4^{2-} in the analysis below.

365   **5. Comparison of event-water fractions estimated from isotopic and chemical tracers**

366   **5.1 Hydrograph separation methodology and uncertainty analysis**

367   To illustrate a potential application of high-frequency isotope and chemical measurements, here we quantify the

368   event-water fractions during the major events captured during the 1-month observation period. We used two-

369   component end-member mixing analysis by applying the conventional mass balance equation (Pinder and Jones,

370   1969):

371    $$F_E = \frac{Q_E}{Q_S} = \frac{C_S - C_P}{C_E - C_P}$$ (3)

372   The fraction of event water relative to total streamflow ($F_E = Q_E/Q_S$) was calculated from the isotope values or

373   solute concentrations in total streamflow (C_S), event precipitation (C_E) and pre-event streamwater (C_P). Here, C_P

374   was obtained for each event from the average of the five streamwater samples immediately before the onset of

375   precipitation. The value of C_E was the incremental, volume-weighted mean (McDonnell et al., 1990) of all

376   precipitation samples that were collected before the respective streamflow sample:

377 $$C_{E,j} = \frac{\sum_{i=k}^{j} P_i C_i}{\sum_{i=k}^{j} P_i} \qquad (4)$$

378 with P_i being the precipitation depth associated with the isotope value (or solute concentration) C_i collected at

379 time i since the starting time k of the precipitation event.

380

381 Uncertainty in the hydrograph separation was quantified with Gaussian error propagation (Genereux, 1998),

382 using calculated standard errors (SE) arising from analytical uncertainties and the temporal variability of the

383 isotope values (or solute concentrations). Because C_E is a volume-weighted mean, the standard error SE_{CE} is

384 calculated with

385 $$SE_{C_{E,j}} = \left[\frac{\sum_{i=k}^{j} P_i (C_i - C_{E,j})^2}{(j-k)\sum_{i=k}^{j} P_i}\right]^{\frac{1}{2}} \qquad (5)$$

386 where $C_{E,j}$ denotes the volume-weighted mean, C_i denotes the ith concentration that comprises that mean, and (j)

387 is the number of samples included in the volume-weighted mean. The standard error of C_S, SE_{CS}, arises from

388 the measurement uncertainties given in Table 1. For SE_{CP}, the same measurement uncertainties are applied, as

389 well as the temporal variability of the five measurements comprising C_P. The standard error of the event-water

390 fraction (SE_{FE}) can then be obtained by Gaussian error propagation:

391 $$SE_{F_E} = \left\{\left[\frac{-1}{C_P - C_E} SE_{C_S}\right]^2 + \left[\frac{C_S - C_E}{(C_P - C_E)^2} SE_{C_P}\right]^2 + \left[\frac{C_P - C_S}{(C_P - C_E)^2} SE_{C_E}\right]^2\right\}^{1/2} \qquad (6)$$

392 Isotope hydrograph separation (IHS) was performed using both $\delta^{18}O$ and δ^2H, whereas chemical hydrograph

393 separation (CHS) was carried out with the three constituents Ca^{2+}, NO_3^- and SO_4^{2-} (Cl^- and Na^+, were not used

394 for CHS due to the influence of road salt at the site) and streamwater EC. EC was used here since several

395 studies apply EC in lieu of chemical concentrations for hydrograph separation, owing to the ease of obtaining

396 continuous EC measurements (e.g., Dzikowski and Jobard, 2012; Matsubayashi et al., 1993; Muñoz-Villers and

397 McDonnell, 2012; Pellerin et al., 2008). As we did not measure EC in precipitation directly, we had to estimate

398 it empirically. For this, we used a standard conversion equation, i.e., the pseudo-linear approach following

399 Sposito (2008), to calculate EC in precipitation from the ionic strength of the major cations and anions in the

400 precipitation samples. We assume that the ion concentrations measured by the IC account for the great majority

401 of the ionic strength. In order to estimate the uncertainty of this method, we also calculated the EC values in

402 streamwater and compared them with the actual measurements of the EC probe in the stream. The (absolute

403 value) difference between the calculated and measured streamwater-EC values averaged 20 μS cm^{-1}.

404

405 For the uncertainty analysis of the calculated event-water fractions, analytical uncertainties in the isotope

406 measurements were assumed to be 0.03 ‰ and 0.17 ‰ for $\delta^{18}O$ and δ^2H, respectively (Section 3.2, Table 1).

407 Relative uncertainties in the IC measurements were $0.006 \cdot C + 0.087$ mg L^{-1} for Ca^{2+}, $0.028 \cdot C + 0.002$ mg L^{-1} for

408 NO_3^- and $0.037 \cdot C + 0.006$ mg L^{-1} for SO_4^{2-}, respectively (where C is concentration in mg L^{-1}; Table 1). For the

409 EC values, a measurement uncertainty of 2 % was assumed for the EC probe based on the specifications given

410 by the EC probe's manufacturer. The assumed uncertainty in the EC values in precipitation was 20 μS cm^{-1}, as

411 calculated above.

412 **5.2 Event-water fractions for eight storm events**

413 Mixing analysis for two end-members, event water and pre-event water, was carried out for eight storm events

414 between 20 February and 8 March 2016, based on isotopic and chemical tracers. Event #8, where precipitation

415 fell partly as snow, was included in the analysis because river discharge and streamwater EC responded within

416 4h after the onset of precipitation (Table 2). Hence, the temporal change in the snowmelt isotopic signal due to

417 fractionation was assumed to be negligible. Two storm events are analyzed in more detail, followed by a

418 general discussion of the hydrograph separation results based on all eight events.

419 **Two storm events**

420 Figures 7 and 8 show the hydrologic, isotopic and chemical responses in streamwater and precipitation

421 duringEvents #1 and #2, respectively. During Event #1, total rainfall was 6.8 mm within 6h, while 11.5 mm

422 rain fell within 13h during Event #2. Antecedent moisture conditions, as inferred from the total rainfall within

423 48 h and 24 h before the event, as well as initial streamwater level, were relatively wet for Event #1 and

424 relatively dry for Event #2 (Table 2).

425

426 For Event #1, $\delta^{18}O$ and δ^2H in streamwater followed the observed patterns in precipitation, i.e. streamwater

427 became isotopically lighter over time. Isotope hydrograph separations (IHS) for this event yielded maximum

428 event-water fractions ($F_{E,max}$) of 80±11 % and 59±14 % for $\delta^{18}O$ and δ^2H, respectively, similar to the results

429 obtained from the chemical tracers Ca^{2+}, NO_3^- and SO_4^{2-} (57±1 %, 65±2 % and 65±3 %) and EC (56±3 %, Fig.

430 7d and e). The larger uncertainties of the IHS compared to CHS can be explained with the large temporal

431 variability of the isotope values in precipitation, which substantially exceeds analytical uncertainty. During

432 Event #1, the fraction of event water increased rapidly after the start of rainfall and declined continuously as

433 stream stage receded. A difference in timing of $F_{E,max}$ was evident for both tracer types (Fig. 7d-e): $F_{E,max}$ based

434 on the chemical tracers occurred 1 h after peak flow, whereas $F_{E,max}$ based on the isotope tracers was roughly 3h

435 delayed, possibly because the isotopic signature in precipitation became lighter as the event progressed.

436 Consequently, if C_S-values at the time of peak flow were used to perform hydrograph separation (Eq. (3)),

437 isotope-based F_E-values would be substantially smaller (i.e., 13±4 % and 15±3 % for $\delta^{18}O$ and δ^2H,

438 respectively) than the $F_{E,max}$-values reported above.

439

440 During Event #2, the solutes in streamwater showed a clear dilution signal (Fig. 8c), similar to Event #1. The

441 isotopic composition in streamwater, by contrast, showed only a very weak and inconsistent response to

442 precipitation. For instance, δ^2H in precipitation increased continuously through the event, whereas δ^2H in

443 streamwater first decreased and then, several hours after the onset of precipitation, began to increase again.

444 Consequently, IHS and CHS yielded substantially different interpretations for Event #2. Maximum event-water

445 fractions based on CHS ranged from 67±1 % (Ca^{2+}) to 82±3 % (SO_4^{2-}), similar to Event #1. In contrast, $F_{E,max}$-

446 values based on IHS ranged from 8±1 % to 15±3 %, indicating that pre-event water was the dominant source of

447 streamwater during peak flow.

448

449   How can such a large discrepancy between the event-water fractions calculated from different environmental

450   tracers be explained? From Fig. 5 it can be seen that precipitation was isotopically lighter than streamwater

451   during the six days leading up to Event #2. Thus, the initial decrease in the δ^{18}O and δ^2H values in streamwater

452   during Event #2 suggests the release of isotopically lighter soilwater and groundwater that were recharged

453   during previous events. An activation of this pre-event water storage might have been triggered by enhanced

454   infiltration after relatively dry antecedent moisture conditions (AMC), compared to the previous event, whereas

455   wet AMC would be more consistent with surface runoff generation. This hypothesis is further supported by the

456   isotopic responses in streamwater during Event #5, another isotopically heavy event with dry AMC, following

457   earlier inputs of isotopically lighter precipitation. In Event #5, small event-water fractions (12±1 % and 21±1 %

458   for δ^{18}O and δ^2H, respectively; Fig. S1) were again obtained, indicating that pre-event water dominated

459   streamflow, similarly to Event #2. And in Event #5, just as in Event #2, the chemical tracers showed strong

460   dilution, leading to an overestimate of the maximum event-water fraction (>40±2 %). In both Event #2 and

461   Event #5, the chemical and isotopic data indicate a large contribution from recent soilwater or groundwater that

462   had not yet become highly mineralized, rather than from either event precipitation or from older groundwater

463   that presumably accounted for most of the pre-event baseflow.

464   **General discussion of hydrograph-separation results**

465   Figure 9 summarizes the estimated event-water fractions for all eight events, based on IHS and CHS, for two

466   points in time during each event: the time with the largest isotopic or chemical response (i.e., $F_{E, max}$) and the

467   time of peak flow. Maximum event-water fractions varied greatly across the eight events (for example, from

468   15±3% to 73±17% based on δ^2H, Fig. 9, Table S1 and S2). Also, within individual events, hydrograph

469   separations based on different isotopic and chemical tracers differed, often by much more than their

470   uncertainties. Inconsistencies between the estimated event-water fractions can be explained with the fact that

471   different tracers are shaped by different hydrochemical processes and flow pathways, and thus may describe

472   different end-members (e.g., Richey et al., 1998; Wels et al., 1991). While stable water isotopes are considered

473   to be ideal conservative tracers, chemical tracers are altered by biogeochemical processes on their way through

474   hydrological systems. These biogeochemical processes also vary over time, as they depend on antecedent

475   conditions and precipitation characteristics. High-frequency analysis of environmental tracers can document

476   this temporal variability, which, in turn, helps to constrain conceptual catchment models. As illustrated by

477   Events #2 and #5, comparing chemical and isotopic tracers can be useful in identifying the temporally variable

478   contributions of different water storages in the subsurface.

479

480   For Event #7, IHS based on δ^{18}O resulted in event-water fractions >100%, which can be explained by the fact

481   that the first precipitation sample of this event was isotopically very similar to the pre-event water signature

482   (C_E=-11.69‰, C_P=-11.09‰). The incremental, volume-weighted mean of the event-water end member was

483   thus isotopically heavier than the streamwater end member, resulting in a smaller difference from the pre-event

484   water end member signature (Eq. 3). Precipitation samples after this first, less-δ^{18}O-depleted sample had an

485   average δ^{18}O value of -16.86±0.73‰ (±standard deviation, n=6). For δ^2H, such a strong effect did not occur

486   and we could obtain reasonable isotope-based hydrograph separation results similar to the chemical hydrograph

487   separation.

488

489   Figure 9 illustrates further that for three events (#2, #5 and #8), estimated event-water fractions for the two

490   isotopes, $\delta^{18}O$ and δ^2H, differed significantly (i.e., by more than twice their pooled uncertainties). These

491   differences did not follow any particular pattern, for instance, $F_E(\delta^{18}O) > F_E(\delta^2H)$ for Event #8, while $F_E(\delta^{18}O)$

492    $< F_E(\delta^2H)$ for Events #2 and #5. Such discrepancies might be caused by temporally variable $\delta^{18}O$-δ^2H relations

493   (d-excess) of contributing water sources (groundwater, soil water, overland flow), resulting in different event-

494   water fractions based on both isotopes. An alternative explanation is that the pre-event streamflow signature

495   (C_P) may not reflect the isotopic signature of the entire pre-event water storage, but only of the components that

496   feed baseflow (e.g., Klaus and McDonnell, 2013). Another way of viewing this problem is that the precipitation

497   event may have mobilized a third pre-event water storage with unknown isotopic composition (e.g., Tetzlaff et

498   al., 2014). This conjecture is strongly supported by the initial shift toward isotopically lighter streamflow early

499   in Event #2, even though the event precipitation was isotopically heavier than the pre-event baseflow. Event #5

500   also showed divergent event-water fractions between the two isotopes, and like Event #2, it also had strongly

501   contrasting pre-event precipitation inputs. Thus, the history of both events suggests that pre-event storage in

502   this catchment was isotopically heterogeneous. This observation is unsurprising, given the pervasive

503   heterogeneity of typical catchments, but a more detailed explanation is not possible with our spatially limited

504   data set. Spatially distributed measurements, such as from groundwater and soil water storages, would help in

505   constraining the individual end-members that contribute to streamflow (e.g., Hangen et al., 2001). Additional

506   high-frequency time series of the groundwater table and soil moisture profiles would allow for documenting the

507   effects of antecedent wetness conditions on the response times and on the activation of different storages at the

508   site. Finally, a spatially distributed precipitation sampling network might help to fully quantify the uncertainty

509   inherent in the event-water signature (e.g., Fischer et al., 2017; Lyon et al., 2009).

510 **5.3 The role of the sampling frequency for capturing hydrological and hydrochemical catchment**
511 **processes**

512   A sampling frequency can be considered optimal when the gain of information from additional measurements is

513   marginal (Kirchner et al., 2004; Neal et al., 2012). With our high-resolution data set we can thus investigate the

514   potential of different sampling frequencies for capturing hydrological and hydrochemical catchment processes,

515   by subsampling the 30 min time series at smaller sampling frequencies, i.e. at 3-hourly, 6-hourly, 12-hourly and

516   daily intervals. To mimic the effects of integrated bulk precipitation samples, we calculated the volume-

517   weighted averages of concentrations and isotope values in precipitation over the corresponding time intervals.

518

519   Figure 10 shows that 3 h sampling frequencies would still be sufficient to capture the isotopic variations in

520   streamwater, including during low-intensity precipitation events. However, the short-term variability within

521   single storm periods, as well as the rapid changes in precipitation isotope values, cannot be resolved at this

522   lower sampling frequency. Thus, even sampling intervals of 3 h can result in a significant loss of information

523   relative to 30 min sampling, and at sampling intervals of 12 h or longer, diurnal fluctuations and some isotopic

524   and chemical responses to low-intensity precipitation events would also be lost. Likewise, the 6 h or 12 h bulk

525   precipitation samples shown in Fig. 10 fail to reflect the large isotopic variability revealed by the 30 min

526   samples.

527

528   To further illustrate the effect of lower sampling frequencies, we performed hydrograph separation with the

529   subsampled data sets, for which illustrative results of the maximum event-water fractions are shown for δ^2H and

530   EC in Fig. 11. With a sampling frequency of 3 h, maximum event-water fractions similar to those for the

531   30 min sampling can still be obtained, except for Events #3 (EC) and #4 (EC) where $F_{E,max}$ is underestimated.

532   Longer sampling intervals (6 h, 12 h) result in much smaller event-water fractions for most events. Because the

533   hydrologic response times in this catchment were only between 0 h and 2.5 h, the durations of the maximum

534   hydrochemical variations were similarly short. Consequently, sampling at longer time intervals increases the

535   risk of missing this critical peak response; if the sample is taken before or after the maximum hydrochemical

536   response, the event-water signal in streamwater (C_S) may be too weak, which will inevitably underestimate

537   event-water fractions, or even lead to unrealistic negative values. Furthermore, the rapid changes observed in

538   precipitation isotopic composition (Fig. 6) suggests that high-frequency measurements are crucial for adequately

539   representing the signature of the event-water end member. Capturing the short-term responses of environmental

540   tracers also helps in better quantifying transit time distributions (e.g., Birkel et al., 2012; Stockinger et al., 2016;

541   Timbe et al., 2015) and in constraining concentration-discharge models (e.g., Stelzer and Likens, 2006; Jones et

542   al., 2012).

543

544   Our data also show that peak flow is not always a reliable predictor for the time when F_E becomes largest. As

545   can be seen for instance during Event #1 (Fig. 7), $F_{E,\,max}$ based on IHS occurred up to 3.0±1.0 h after peak flow.

546   The timing of peak flow and the $F_{E,\,max}$ values for chemical and isotope tracers coincided for only four events

547   (i.e., #2, #6, #7, #8). During the remaining events, the tracer signal showed the strongest responses up to

548   2.5±1.0 h after peak flow, indicating that the time window for sample collection at our site must extend more

549   than 3 h before and after peak flow in order to capture the whole range of event water dynamics. In the case of

550   snowmelt Event #8, when the maximum EC response occurred 5 h before peak flow, an even longer sampling

551   period would be required in order to capture unusual events such as the inflow of water contaminated by road

552   salt.

553   **6 Concluding remarks**

554   This paper presents the first field hydrology application of Picarro's Continuous Water Sampler (CWS) module,

555   which was coupled to a L2130-*i* Wavelength Scanned-Cavity ring-down Spectrometer to measure δ^{18}O and δ^2H

556   in streamwater and precipitation at a temporal resolution of 30 min. We combined this real-time isotope

557   analysis system with a dual-channel ion chromatograph for synchronous analysis of major cations and anions.

558   Good instrument performance and high measurement precision could be achieved during continuous 48-hour

559   laboratory experiments and a 28-day deployment in the field at a small, partly urbanized catchment in central

560   Switzerland.

561

562   Problematic issues such as sample degradation during storage and transportation, which arise in conventional

563   sampling for catchment tracer studies, become irrelevant with the system presented here. At the same time,

564   potential registration errors arising during the collection and handling of large numbers of water samples are

565 avoided. Conversely, two major limitations of the coupled isotope analyzer / IC system are its high cost and the
566 need for line power, constraining its use in remote locations. However, laboratory analysis of conventionally
567 collected grab samples is also cost-intensive, and autosamplers used in conventional sampling schemes also
568 require a reliable energy supply (though at much lower power levels).
569
570 The results of the high-frequency analysis system are presented here to provide a proof-of-concept and an
571 illustration of its functionality at the field, rather than to fully document the hydrological and biogeochemical
572 processes at this field site. A more detailed interpretation would require additional measurements of soilwater
573 and groundwater isotopes and chemistry, in order to better constrain the end-members in the mixing analysis.
574 Nevertheless, our one-month field experiment demonstrates the marked short-term variability of several natural
575 tracers in a small, highly dynamic watershed. The hydrograph separation exercise clearly showed that long-
576 term, high-frequency isotopic and chemical analyses are essential for capturing the "unusual but informative"
577 events that shed light on catchment storage and flow processes. We further showed that the right timing for
578 capturing peak event-water contributions can easily be missed with conventional grab sampling strategies at
579 time intervals longer than 3 h, resulting in an underestimation of the event-water fraction. In addition, the
580 relative timing of the isotopic and chemical responses was highly variable, demonstrating the challenge of
581 capturing the right moments with episodic snapshot campaigns or long-term monitoring with daily, weekly, or
582 even monthly sampling intervals.
583
584 As was shown here and elsewhere (e.g., Kirchner, 2003), short-term responses of streamflow and environmental
585 tracers may follow distinctly different patterns, which helps in constraining streamflow-generation mechanisms
586 and quantifying short transit times. Thus, high-frequency isotopic and chemical measurements also have great
587 potential for catchment model validation. Potential future applications of the system could include sites with
588 rapid hydrologic responses, such as urban streams (e.g., Jarden et al., 2016; Jefferson et al., 2015; Soulsby et
589 al., 2014), wastewater and drinking water systems (e.g., Houhou et al., 2010; Kracht et al., 2007) or agricultural
590 catchments with artificial drainage networks (e.g., Doppler et al., 2012; Heinz et al., 2014). By eliminating
591 errors associated with the handling, transportation and storage of individual bottles, our analysis system may
592 also achieve better precision than conventional field sampling followed by laboratory analyses. As a result, our
593 system may be able to detect subtle isotopic and biogeochemical signals (associated with, e.g., evaporation
594 effects or in-stream biological processes) that would be missed by conventional approaches to sampling and
595 analysis. Thus, this system can potentially shed new light on the linkages between hydrological, biological, and
596 geochemical processes.

597 **Acknowledgements**

598 We thank Anton Burkhardt and the facilities staff of the Swiss Federal Institute for Forest, Snow and Landscape
599 Research (WSL) for logistical support, and Matthias Haeni from the Long-term Forest Ecosystem Research
600 Programme (LWF) at WSL for providing air temperature data. We also thank Barbara Herstritt of the isotope
601 laboratory at the University Freiburg (Germany) for the analysis of the isotope reference standards, as well as
602 Kate Dennis and David Kim-Hak of Picarro Inc. (Santa Clara, CA, USA) for technical advice.

References

Aubert, A. H., Gascuel-Odoux, C., Gruau, G., Akkal, N., Faucheux, M., Fauvel, Y., Grimaldi, C., Hamon, Y., Jaffrezic, A., Lecoz-Boutnik, M., Molenat, J., Petitjean, P., Ruiz, L., and Merot, P.: Solute transport dynamics in small, shallow groundwater-dominated agricultural catchments: insights from a high-frequency, multisolute 10 yr-long monitoring study, Hydrol. Earth Syst. Sci., 17, 1379-1391, 10.5194/hess-17-1379-2013, 2013.

Aubert, A. H., and Breuer, L.: New seasonal shift in in-stream diurnal nitrate cycles identified by mining high-frequency data, PLoS ONE, 11, 10.1371/journal.pone.0153138, 2016.

Bende-Michl, U., and Hairsine, P. B.: A systematic approach to choosing an automated nutrient analyser for river monitoring, Journal of Environmental Monitoring, 12, 127-134, 2010.

Benettin, P., Kirchner, J. W., Rinaldo, A., and Botter, G.: Modeling chloride transport using travel time distributions at Plynlimon, Wales, Water Resour. Res., 51, 3259-3276, 10.1002/2014WR016600, 2015.

Berman, E. S. F., Gupta, M., Gabrielli, C., Garland, T., and McDonnell, J. J.: High-frequency field-deployable isotope analyzer for hydrological applications, Water Resour. Res., 45, 10.1029/2009wr008265, 2009.

Birkel, C., Soulsby, C., Tetzlaff, D., Dunn, S., and Spezia, L.: High-frequency storm event isotope sampling reveals time-variant transit time distributions and influence of diurnal cycles, Hydrol. Process., 26, 308-316, 10.1002/hyp.8210, 2012.

Buso, D. C., Likens, G. E., and Eaton, J. S.: Chemistry of precipitation, streamwater, and lakewater from the Hubbard Brook Ecosystem Study: a record of sampling protocols and analytical procedures, USDA Forest Service, Northeastern Research Station, USDA Forest Service, Newtown Square, PA., Gen. Tech. Rep. NE-275, 52pp, 2000.

Craig, H.: Isotopic variations in meteoric waters, Science, 133, 1702-1703, 1961.

Darling, W. G., and Bowes, M. J.: A long-term study of stable isotopes as tracers of processes governing water flow and quality in a lowland river basin: the upper Thames, UK, Hydrol. Process., 30, 2178-2195, 10.1002/hyp.10779, 2016.

Doppler, T., Camenzuli, L., Hirzel, G., Krauss, M., Luck, A., and Stamm, C.: Spatial variability of herbicide mobilisation and transport at catchment scale: insights from a field experiment, Hydrol. Earth Syst. Sci., 16, 1947-1967, 10.5194/Hess-16-1947-2012, 2012.

Dzikowski, M., and Jobard, S.: Mixing law versus discharge and electrical conductivity relationships: application to an alpine proglacial stream, Hydrol. Process., 26, 2724-2732, Doi 10.1002/Hyp.8366, 2012.

Fischer, B. M. C., van Meerveld, I., and Seibert, J.: Spatial variability in the isotopic composition of rainfall in a small headwater catchment and its effect on hydrograph separation, Journal of Hydrology, http://dx.doi.org/10.1016/j.jhydrol.2017.01.045, 2017.

Genereux, D.: Quantifying uncertainty in tracer-based hydrograph separations, Water Resour. Res., 34, 915-919, 1998.

GIS-ZH: Geographisches Informationssystem des Kantons Zürich (GIS-ZH), Amt für Raumentwicklung, Abteilung Geoinformation, GIS-Produkte GIS-Browser, Map, available at: http://maps.zh.ch/, last access: 4 October 2016, 2016.

Gupta, P., Noone, D., Galewsky, J., Sweeney, C., and Vaughn, B. H.: Demonstration of high-precision continuous measurements of water vapor isotopologues in laboratory and remote field deployments using wavelength-scanned cavity ring-down spectroscopy (WS-CRDS) technology, Rapid Commun Mass Sp, 23, 2534-2542, 10.1002/rcm.4100, 2009.

Halliday, S. J., Skeffington, R. A., Wade, A. J., Neal, C., Reynolds, B., Norris, D., and Kirchner, J. W.: Upland streamwater nitrate dynamics across decadal to sub-daily timescales: a case study of Plynlimon, Wales, Biogeosciences, 10, 8013-8038, 2013.

Hangen, E., Lindenlaub, M., Leibundgut, C., and von Wilpert, K.: Investigating mechanisms of stormflow generation by natural tracers and hydrometric data: a small catchment study in the Black Forest, Germany, Hydrol. Process., 15, 183-199, 2001.

Harman, C. J.: Time-variable transit time distributions and transport: Theory and application to storage-dependent transport of chloride in a watershed, Water Resour. Res., 51, 1-30, 10.1002/2014WR015707, 2015.

5   Hayashi, M., Vogt, T., Mächler, L., and Schirmer, M.: Diurnal fluctuations of electrical conductivity in a pre-alpine river: Effects of photosynthesis and groundwater exchange, Journal of Hydrology, 450, 93-104, Doi 10.1016/J.Jhydrol.2012.05.020, 2012.

Heinz, E., Kraft, P., Buchen, C., Frede, H. G., Aquino, E., and Breuer, L.: Set Up of an Automatic Water Quality Sampling System in Irrigation Agriculture, Sensors-Basel, 14, 212-228, 10.3390/S140100212, 2014.

Herbstritt, B., Gralher, B., and Weiler, M.: Continuous in situ measurements of stable isotopes in liquid water, Water Resour. Res., 48,
10   10.1029/2011wr011369, 2012.

Houhou, J., Lartiges, B. S., France-Lanord, C., Guilmette, C., Poix, S., and Mustin, C.: Isotopic tracing of clear water sources in an urban sewer: A combined water and dissolved sulfate stable isotope approach, Water Research, 44, 256-266, 10.1016/j.watres.2009.09.024, 2010.

Jarden, K. M., Jefferson, A. J., and Grieser, J. M.: Assessing the effects of catchment-scale urban green infrastructure retrofits on
15   hydrograph characteristics, Hydrol. Process., 30, 1536-1550, 10.1002/hyp.10736, 2016.

Jasechko, S., Kirchner, J. W., Welker, J. M., and McDonnell, J. J.: Substantial proportion of global streamflow less than three months old, Nature Geoscience, 9, 126-129, 10.1038/Ngeo2636, 2016.

Jefferson, A. J., Bell, C. D., Clinton, S. M., and McMillan, S. K.: Application of isotope hydrograph separation to understand contributions of stormwater control measures to urban headwater streams, Hydrol. Process., 29, 5290-5306, 10.1002/hyp.10680, 2015.

20   Jones, A. S., Horsburgh, J. S., Mesner, N. O., Ryel, R. J., and Stevens, D. K.: Influence of Sampling Frequency on Estimation of Annual Total Phosphorus and Total Suspended Solids Loads, J. Am. Water Resour. Assoc., 48, 1258-1275, 10.1111/j.1752-1688.2012.00684.x, 2012.

Kendall, C., and McDonnell, J. J.: Isotope tracers in catchment hydrology, Elsevier, Amsterdam ; New York, xxix, 839 p. pp., 1998.

Kirchner, J. W.: A double paradox in catchment hydrology and geochemistry, Hydrol. Process., 17, 871-874, 10.1002/Hyp.5108, 2003.

25   Kirchner, J. W., Feng, X. H., Neal, C., and Robson, A. J.: The fine structure of water-quality dynamics: the (high-frequency) wave of the future, Hydrol. Process., 18, 1353-1359, 10.1002/Hyp.5537, 2004.

Kirchner, J. W., and Neal, C.: Universal fractal scaling in stream chemistry and its implications for solute transport and water quality trend detection, P Natl Acad Sci USA, 110, 12213-12218, 10.1073/Pnas.1304328110, 2013.

Klaus, J., and McDonnell, J. J.: Hydrograph separation using stable isotopes: Review and evaluation, Journal of Hydrology, 505, 47-64,
30   10.1016/j.jhydrol.2013.09.006, 2013.

Kracht, O., Gresch, M., and Gujer, W.: A Stable Isotope Approach for the Quantification of Sewer Infiltration, Environmental Science & Technology, 41, 5839-5845, 10.1021/es062960c, 2007.

Leibundgut, C., and Seibert, J.: Tracer Hydrology, in: The Science of Hydrology, edited by: Uhlenbrook, S., Treatise on Water Science, Elsevier, Amsterdam, 215-236, 2011.

35   Lyon, S. W., Desilets, S. L. E., and Troch, P. A.: Characterizing the response of a catchment to an extreme rainfall event using hydrometric and isotopic data, Water Resour. Res., 44, 10.1029/2007wr006259, 2008.

Lyon, S. W., Desilets, S. L. E., and Troch, P. A.: A tale of two isotopes: differences in hydrograph separation for a runoff event when using delta D versus delta O-18, Hydrol. Process., 23, 2095-2101, 10.1002.hyp.7326, 2009.

Matsubayashi, U., Velasquez, G. T., and Takagi, F.: Hydrograph separation and flow analysis by specific electrical conductance of water, Journal of Hydrology, 152, 179-199, 10.1016/0022-1694(93)90145-Y, 1993.

5 McDonnell, J. J., Bonell, M., Stewart, M. K., and Pearce, A. J.: Deuterium Variations in Storm Rainfall - Implications for Stream Hydrograph Separation, Water Resour. Res., 26, 455-458, 10.1029/WR026i003p00455, 1990.

McGlynn, B. L., and McDonnell, J. J.: Quantifying the relative contributions of riparian and hillslope zones to catchment runoff, Water Resour. Res., 39, 10.1029/2003wr002091, 2003.

Moerman, J. W., Cobb, K. M., Adkins, J. F., Sodemann, H., Clark, B., and Tuen, A. A.: Diurnal to interannual rainfall δ18O variations in
10 northern Borneo driven by regional hydrology, Earth and Planetary Science Letters, 369–370, 108-119, http://dx.doi.org/10.1016/j.epsl.2013.03.014, 2013.

Munksgaard, N. C., Wurster, C. M., and Bird, M. I.: Continuous analysis of delta O-18 and delta D values of water by diffusion sampling cavity ring-down spectrometry: a novel sampling device for unattended field monitoring of precipitation, ground and surface waters, Rapid Commun Mass Sp, 25, 3706-3712, 10.1002/rcm.5282, 2011.

15 Munksgaard, N. C., Wurster, C. M., Bass, A., and Bird, M. I.: Extreme short-term stable isotope variability revealed by continuous rainwater analysis, Hydrol. Process., 26, 3630-3634, 10.1002/hyp.9505, 2012.

Muñoz-Villers, L. E., and McDonnell, J. J.: Runoff generation in a steep, tropical montane cloud forest catchment on permeable volcanic substrate, Water Resour. Res., 48, n/a-n/a, 10.1029/2011WR011316, 2012.

Neal, C., Reynolds, B., Norris, D., Kirchner, J. W., Neal, M., Rowland, P., Wickham, H., Harman, S., Armstrong, L., Sleep, D., Lawlor,
20 A., Woods, C., Williams, B., Fry, M., Newton, G., and Wright, D.: Three decades of water quality measurements from the Upper Severn experimental catchments at Plynlimon, Wales: an openly accessible data resource for research, modelling, environmental management and education, Hydrol. Process., 25, 3818-3830, 10.1002/hyp.8191, 2011.

Neal, C., Reynolds, B., Rowland, P., Norris, D., Kirchner, J. W., Neal, M., Sleep, D., Lawlor, A., Woods, C., Thacker, S., Guyatt, H., Vincent, C., Hockenhull, K., Wickham, H., Harman, S., and Armstrong, L.: High-frequency water quality time series in precipitation and
25 streamflow: From fragmentary signals to scientific challenge, Sci Total Environ, 434, 3-12, http://dx.doi.org/10.1016/j.scitotenv.2011.10.072, 2012.

Pangle, L. A., Klaus, J., Berman, E. S. F., Gupta, M., and McDonnell, J. J.: A new multisource and high-frequency approach to measuring δ2H and δ18O in hydrological field studies, Water Resour. Res., 49, 7797-7803, 10.1002/2013WR013743, 2013.

Pellerin, B. A., Wollheim, W. M., Feng, X., and Vörörsmarty, C. J.: The application of electrical conductivity as a tracer for hydrograph
30 separation in urban catchments, Hydrol. Process., 22, 1810-1818, 10.1002/hyp.6786, 2008.

Pinder, G. F., and Jones, J. F.: Determination of the ground-water component of peak discharge from the chemistry of total runoff, Water Resour. Res., 5, 438-445, 10.1029/WR005i002p00438, 1969.

Richey, D. G., McDonnell, J. J., Erbe, M. W., and Hurd, T. M.: Hydrograph separations based on chemical and isotopic concentrations: A critical appraisal of published studies from New Zealand, North America and Europe, Journal of Hydrology New Zealand, 37, 95-111,
35 1998.

Riml, J., and Worman, A.: Spatiotemporal decomposition of solute dispersion in watersheds, Water Resour. Res., 51, 2377-2392, 10.1002/2014WR016385, 2015.

Rode, M., Angelstein, S. H. N., Anis, M. R., Borchardt, D., and Weitere, M.: Continuous In-Stream Assimilatory Nitrate Uptake from High Frequency Sensor Measurements, Environmental Science & Technology, 50, 5685-5694, 2016a.

Rode, M., Wade, A. J., Cohen, M. J., Hensley, R. T., Bowes, M. J., Kirchner, J. W., Arhonditsis, G. B., Jordan, P., Kronvang, B., Halliday, S. J., Skeffington, R. A., Rozemeijer, J. C., Aubert, A. H., Rinke, K., and Jomaa, S.: Sensors in the Stream: The High-Frequency Wave of the Present, Environmental Science & Technology, 50, 10297-10307, 10.1021/acs.est.6b02155, 2016b.

Schaub, M., Dobbertin, M., Krauchi, N., and Dobbertin, M. K.: Preface-long-term ecosystem research: understanding the present to shape the future, Environ Monit Assess, 174, 1-2, 2011.

Soulsby, C., Birkel, C., and Tetzlaff, D.: Assessing urbanization impacts on catchment transit times, Geophysical Research Letters, 41, 442-448, 2014.

Sposito, G.: The chemistry of soils, 2nd ed., Oxford University Press, Oxford; New York, xii, 329 p. pp., 2008.

Stelzer, R. S., and Likens, G. E.: Effects of sampling frequency on estimates of dissolved silica export by streams: The role of hydrological variability and concentration-discharge relationships, Water Resour. Res., 42, 10.1029/2005WR004615, 2006.

Stockinger, M. P., Bogena, H. R., Lücke, A., Diekkrüger, B., Cornelissen, T., and Vereecken, H.: Tracer sampling frequency influences estimates of young water fraction and streamwater transit time distribution, Journal of Hydrology, 541, Part B, 952-964, http://dx.doi.org/10.1016/j.jhydrol.2016.08.007, 2016.

Tetzlaff, D., Birkel, C., Dick, J., Geris, J., and Soulsby, C.: Storage dynamics in hydropedological units control hillslope connectivity, runoff generation, and the evolution of catchment transit time distributions, Water Resour. Res., 50, 969-985, 2014.

Timbe, E., Windhorst, D., Celleri, R., Timbe, L., Crespo, P., Frede, H. G., Feyen, J., and Breuer, L.: Sampling frequency trade-offs in the assessment of mean transit times of tropical montane catchment waters under semi-steady-state conditions, Hydrol. Earth Syst. Sci., 19, 1153-1168, 10.5194/hess-19-1153-2015, 2015.

Tweed, S., Munksgaard, N., Marc, V., Rockett, N., Bass, A., Forsythe, A. J., Bird, M. I., and Leblanc, M.: Continuous monitoring of stream delta O-18 and delta H-2 and stormflow hydrograph separation using laser spectrometry in an agricultural catchment, Hydrol. Process., 30, 648-660, 10.1002/hyp.10689, 2016.

Vitvar, T., and Balderer, W.: Estimation of mean water residence times and runoff generation by O-18 measurements in a pre-Alpine catchment (Rietholzbach, eastern Switzerland), Applied Geochemistry, 12, 787-796, 1997.

Weiler, M., Scherrer, S., Naef, F., and Burlando, P.: Hydrograph separation of runoff components based on measuring hydraulic state variables, tracer experiments, and weighting methods, Integrated Methods in Catchment Hydrology: Tracer, Remote Sensing and New Hydrometric Techniques, 249-255, 1999.

Wels, C., Cornett, R. J., and Lazerte, B. D.: Hydrograph Separation - a Comparison of Geochemical and Isotopic Tracers, Journal of Hydrology, 122, 253-274, 10.1016/0022-1694(91)90181-G, 1991.

Tables

Table 1: Average isotope values and solute concentrations, as well as standard deviations (and relative standard deviations RSD) of three water samples analyzed during two different 48-hour laboratory experiments with the isotope analyzer and IC, respectively. In Fiji bottled water, tap water and nanopure water, concentrations of F^-, Li^+, K^+, NH_4^+ and PO_4^{3-} were mostly below the limit of quantification (LOQ), and thus were not included in the table. The calculation of the average memory coefficient is described in the text (Eq. (1)). The uncertainties of the IC measurements were obtained by simple linear regression analysis of the average value and the standard deviation of the respective constituent.

	Isotope analyzer 48-hour laboratory experiment		IC 48-hour laboratory experiment					
	$\delta^{18}O$	δ^2H	Na^+	Mg^{2+}	Ca^{2+}	Cl^-	NO_3^-	SO_4^{2-}
Limit of quantification (LOQ) (mg L^{-1})	-	-	0.1	0.1	0.1	0.05	0.05	0.05
Measurement uncertainty (‰) or (mg L^{-1})	0.03	0.17	0.053+ 0.005·C	0.008+ 0.006·C	0.087+ 0.009·C	0.027+ 0.003·C	0.028+ 0.002·C	0.037+ 0.006·C
Water sample	**Fiji bottled water**		**Fiji bottled water**					
Number of measurements	12	12	10	10	10	10	10	10
Average value (‰) or (mg L^{-1})	-4.86	-35.89	21.6	15.7	24.3	9.69	1.05	1.56
Standard deviation (‰) or (mg L^{-1})	0.06	0.26	0.1	0.1	0.3	0.06	0.05	0.03
RSD (%)	-	-	0.5	0.4	1.1	0.60	4.3	1.80
Linear drift (mean±standard error) (‰ 24h^{-1}) or (mg L^{-1} 24h^{-1})	-0.009±0.008	0.133±0.040	0.129± 0.056 [a]	0.058± 0.036 [b]	0.093± 0.160 [c]	0.088± 0.019	-0.078± 0.008	0.045± 0.007
Water sample	**Tap water**		**Tap water**					
Number of measurements	34	34	18	18	18	18	18	18
Average value (‰) or (mg L^{-1})	-9.40	-68.55	10.9	34.4	133.2	12.41	4.96	17.29
Standard deviation (‰) or (mg L^{-1})	0.03	0.12	0.2	0.2	1.3	0.057	0.03	0.14
RSD (%)	-	-	1.6	0.6	1.0	0.5	0.7	0.8
Water sample	**Nanopure water**		**Nanopure water (last sample)**					
Number of measurements	43	43	27	27	27	27	27	27
Average value (‰) or (mg L^{-1})	-9.44	-68.67	<LOQ	0.1	0.6	<LOQ	<LOQ	0.09
Standard deviation (‰) or (mg L^{-1})	0.02	0.18	0.02	0.003	0.1	0.03	0.02	0.05
Carryover (%)	0.9	1.2	2.8	3.3	3.8	2.1	1.9	2.3

[a] $p > 0.05$
[b] $p > 0.15$
[c] $p > 0.50$

Table 2: Characteristics of precipitation events and antecedent moisture conditions during the field experiment. Initial stream stage is used here as a proxy for initial discharge.

Event	Start of event	Total precipitation (mm)	Total precipitation until peak flow (mm)	Response time (h:min)	48h antecedent precipitation (mm)	24h antecedent precipitation (mm)	Initial stream stage (m)
#1	14 February 2016 11:00	5.8	2.2	01:10	8.3	2.7	0.44
#2	20 February 2016 10:00	11.5	8.8	00:30	1.9	0.5	0.36
#3	23 February 2016 8:00	5.8	3.5	00:00	0.8	0.8	0.37
#4	24 February 2016 15:00	14.3	8.1	01:00	6.6	5.0	0.41
#5	29 February 2016 13:00	10.5	2.0	00:00	0.0	0.0	0.38
#6	2 March 2016 13:00	8.7	6.8	01:10	12.3	1.9	0.46
#7	5 March 2016 4:00	11.5	9.4	02:10	4.6	0.9	0.45
#8	7 March 2016 23:00	8.4	8.4	02:30	0.6	0.0	0.45

Figures
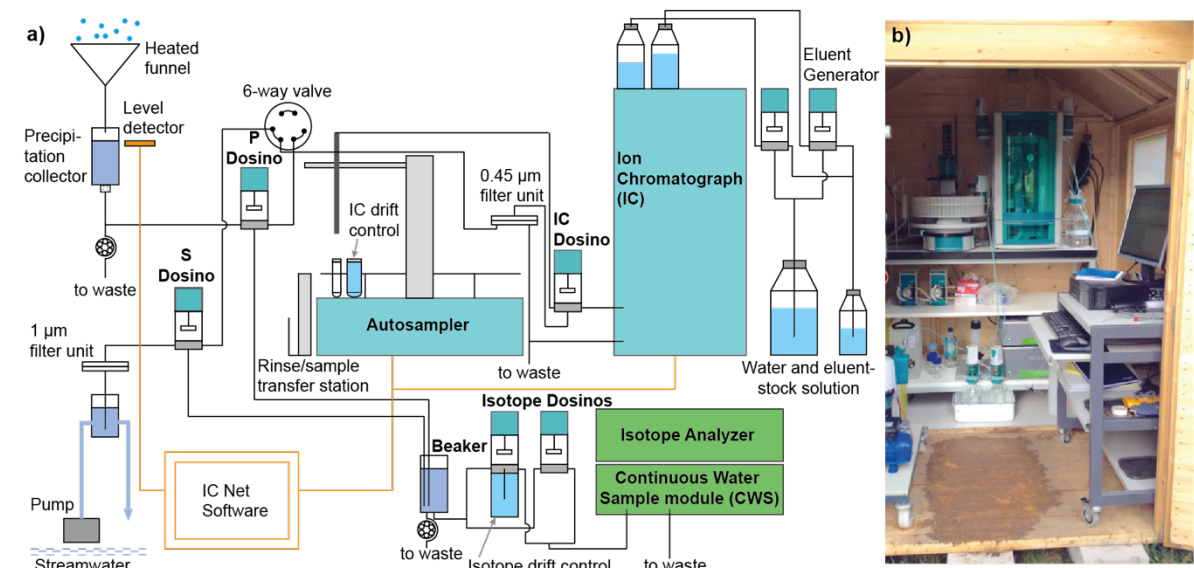
Figure 1: a) Schematic overview of the coupled isotope analyzer / IC- system for the collection and analysis of streamwater and precipitation samples. Components of the sample distribution and the IC are shown in blue, while the isotope analyzer with CWS is shown in green. Panel b) shows a photo of the coupled isotope analyzer / IC- system in the wooden hut during the field experiment.
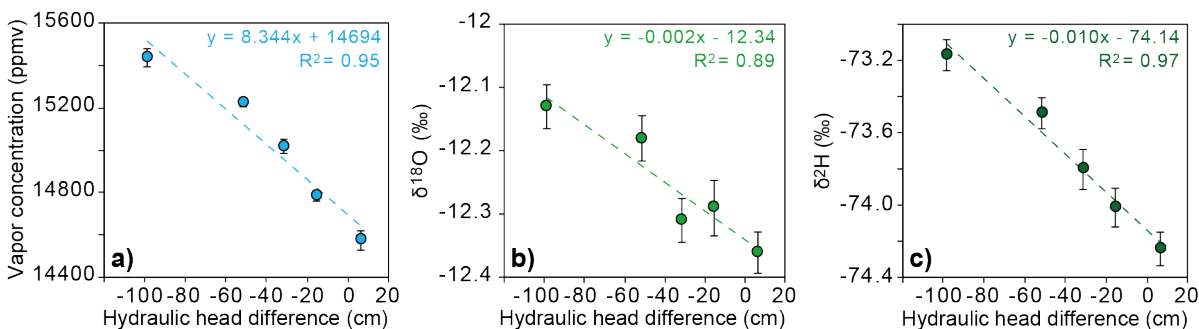
Figure 2: Experiment showing the isotope effects of sample injection into the continuous water sampler (CWS). Panel a) shows measured vapor concentrations, and panels b) and c) show the raw, uncalibrated isotope values of a single water sample (nanopure water) as a function of the hydraulic head difference between the water level in the sample bottle and the waste outlet. Negative values of the hydraulic head difference indicate that the sample source was located below the waste outlet of the CWS.
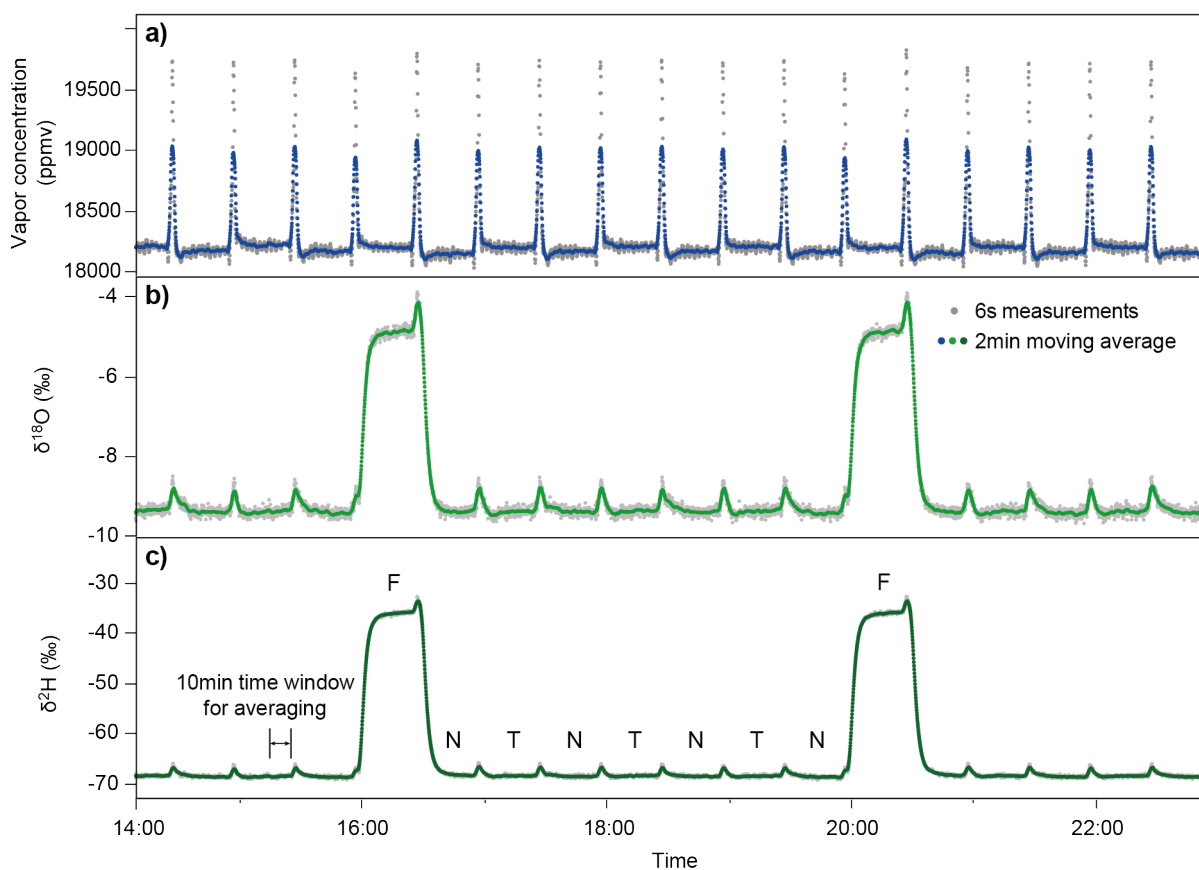
Figure 3: Nine-hour excerpt showing raw, uncalibrated data of vapor concentrations (panel a)) and isotope measurements (panels b) and c)) in tap water (T), nanopure water (N) and Fiji bottled water (F) during the 48-hour laboratory experiment. Samples were injected alternately with two Dosinos for 30min each at a flow rate of 1 mL min^{-1}.
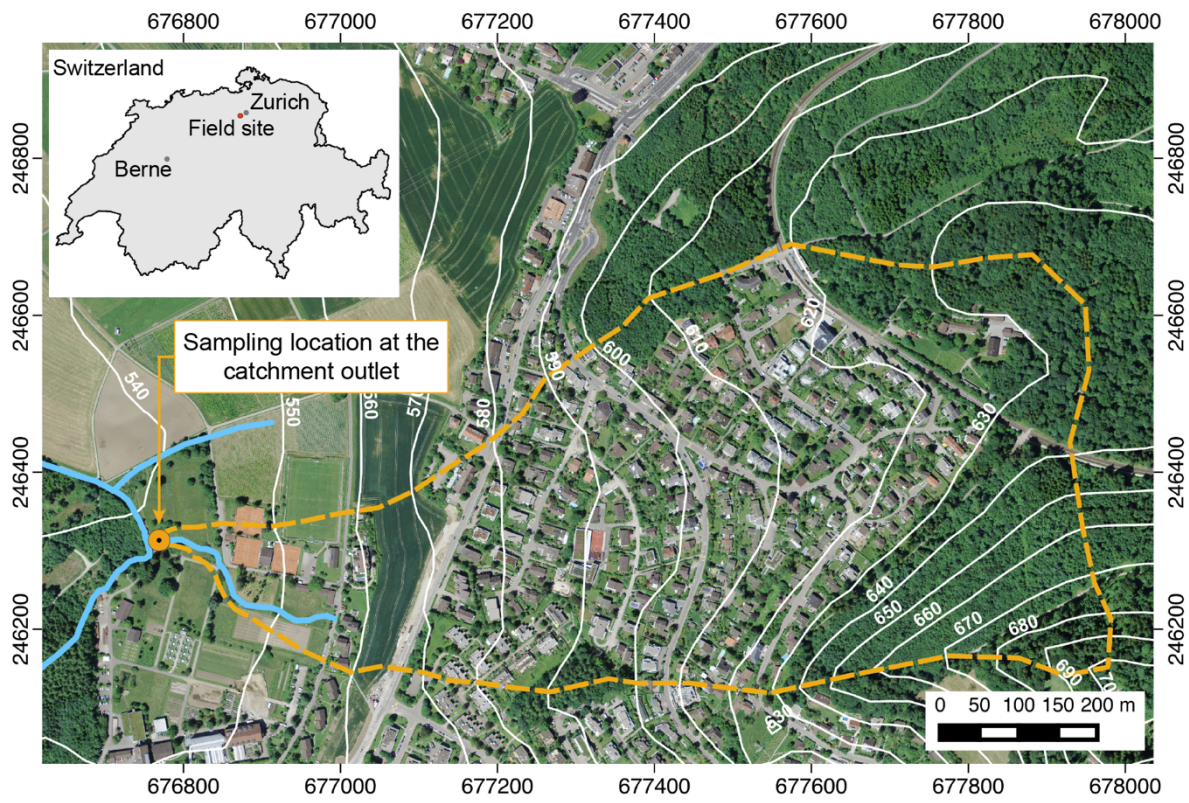
Figure 4: Location of the field site at a small creek on the property of the Swiss Federal Institute for Forest, Snow and Landscape Research (WSL) near Zurich, Switzerland. Catchment boundaries are approximate.
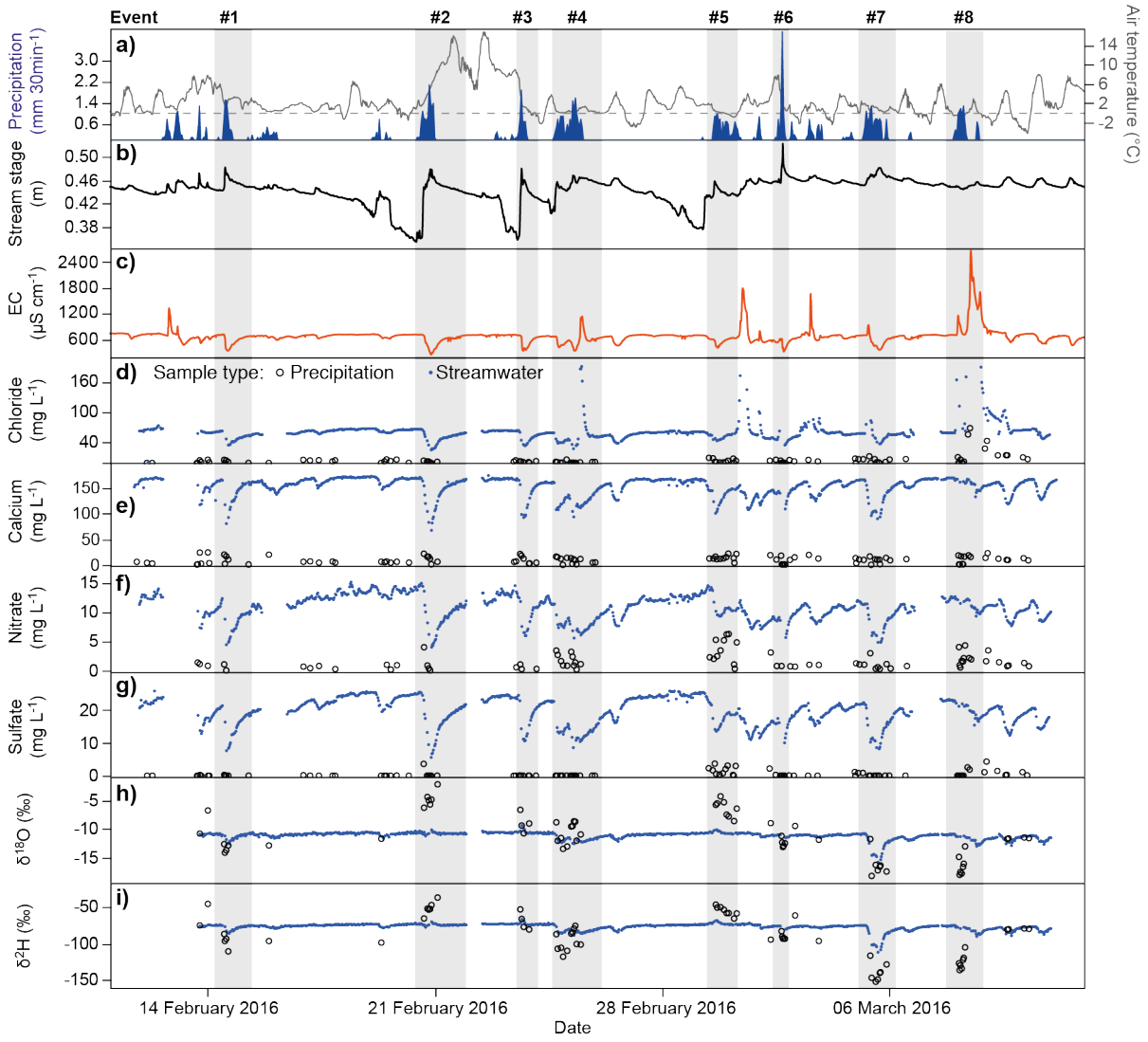
Figure 5: Time series of a) precipitation and air temperature, as well as b) stream stage at the field site during the four-week study period. Panel c) shows streamwater EC, whereas panels d – g) show the chloride, calcium, nitrate and sulfate concentrations, respectively. Panels h) and i) show the isotopic compositions of precipitation and streamwater samples. Streamwater samples are shown by blue dots and precipitation samples are shown by open circles. Vertical grey bars indicate the periods of the eight precipitation events used for hydrograph separation.
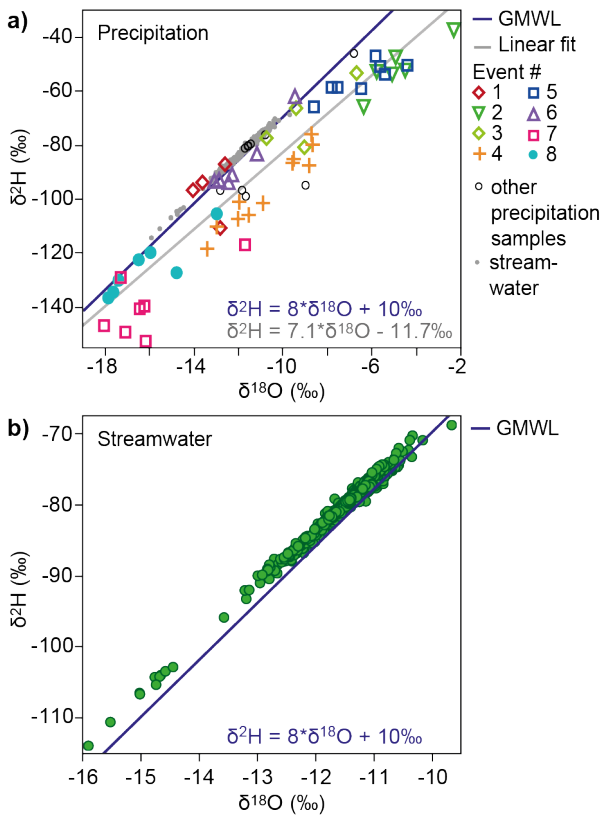
Figure 6: Dual-isotope plot of all δ^{18}O and δ^{2}H values measured in a) precipitation and b) streamwater during the field experiment. Streamwater samples are also plotted in grey in the upper panel for comparison (note the difference in scales). The global meteoric water line (GWML, Craig (1961)) and the linear fit to the precipitation data are shown in blue and in grey, respectively.
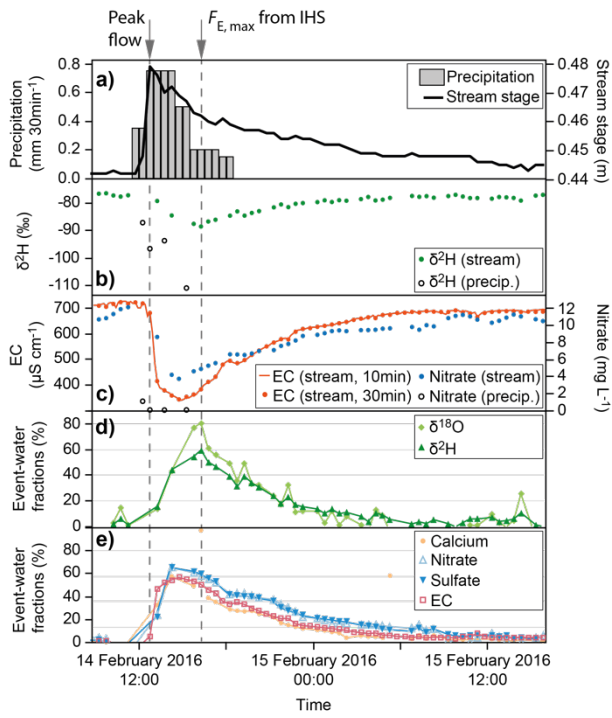
Figure 7: Precipitation Event #1 together with the a) hydrologic, b) isotopic and c) chemical responses in streamwater. Panels d) and e) show the fractions of event-water based on isotopic and chemical hydrograph separation, respectively, which are similar for both types of tracers. However, the timing of the maximum event-water fraction ($F_{E,max}$) differs, with the isotopes indicating the largest contribution of event water around 3h after the peak flow was reached. In panel e), gaps in the F_E time series based on calcium concentrations are due to measurement outliers.
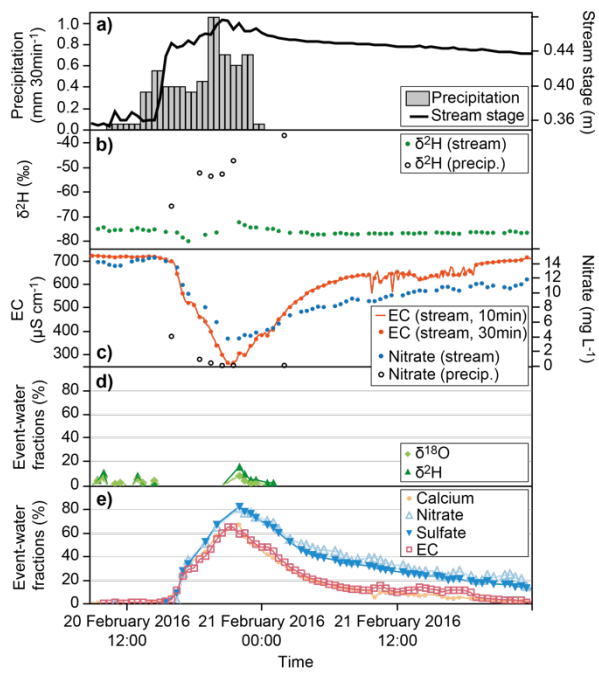
Figure 8: Precipitation Event #2 and the a) hydrologic, b) isotopic and c) chemical responses in streamwater. Panels d) and e) show the fractions of event water (F_E) based on isotopic and chemical hydrograph separation. Chemical tracers greatly exaggerate the event-water fraction.
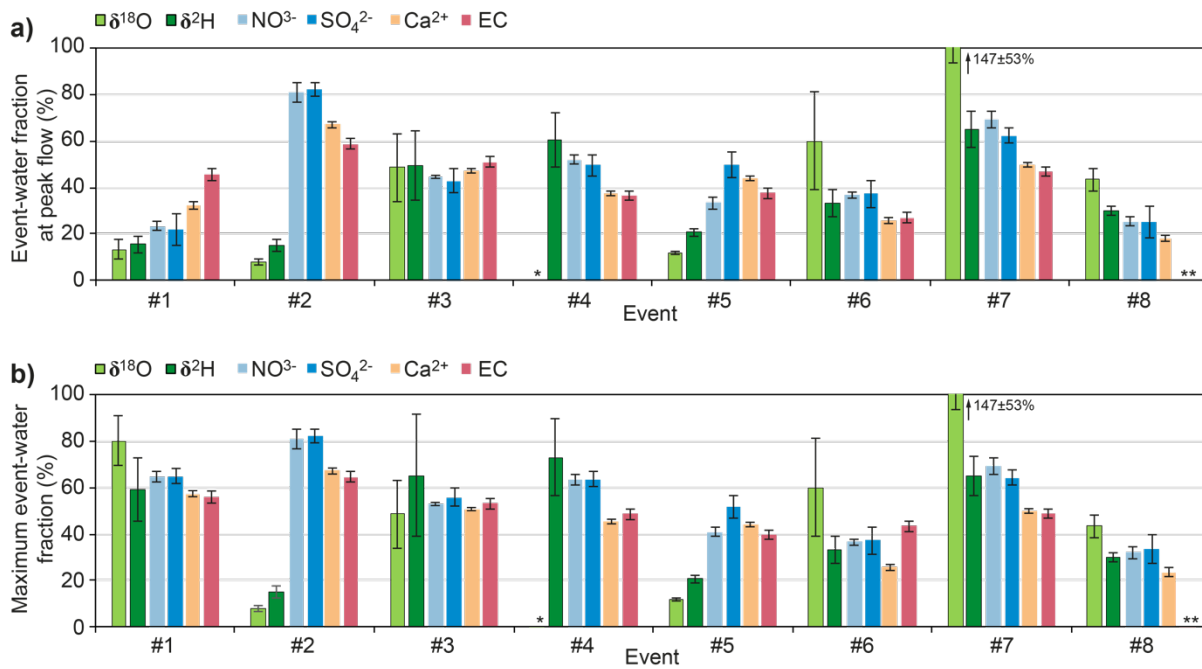
Figure 9: Event-water fractions (F_E) based on isotopic and chemical hydrograph separation for eight storm events. Panel a) shows F_E during peak flow, and panel b) shows the maximum event-water fractions ($F_{E,max}$) of each event. Unrealistic F_E and $F_{E,max}$ values based on $\delta^{18}O$ were obtained for Event #4 because the isotopic signatures in precipitation and pre-event streamwater were too similar (*). For Event #8, wash-off of road salt resulted in unrealistic F_E and $F_{E,max}$ values based on EC, i.e. -96±6% and -95±6% (**), respectively. The larger uncertainties of the IHS results compared to CHS can be explained with the large temporal variability of the isotope values in precipitation, which substantially exceeds analytical uncertainty during most events.
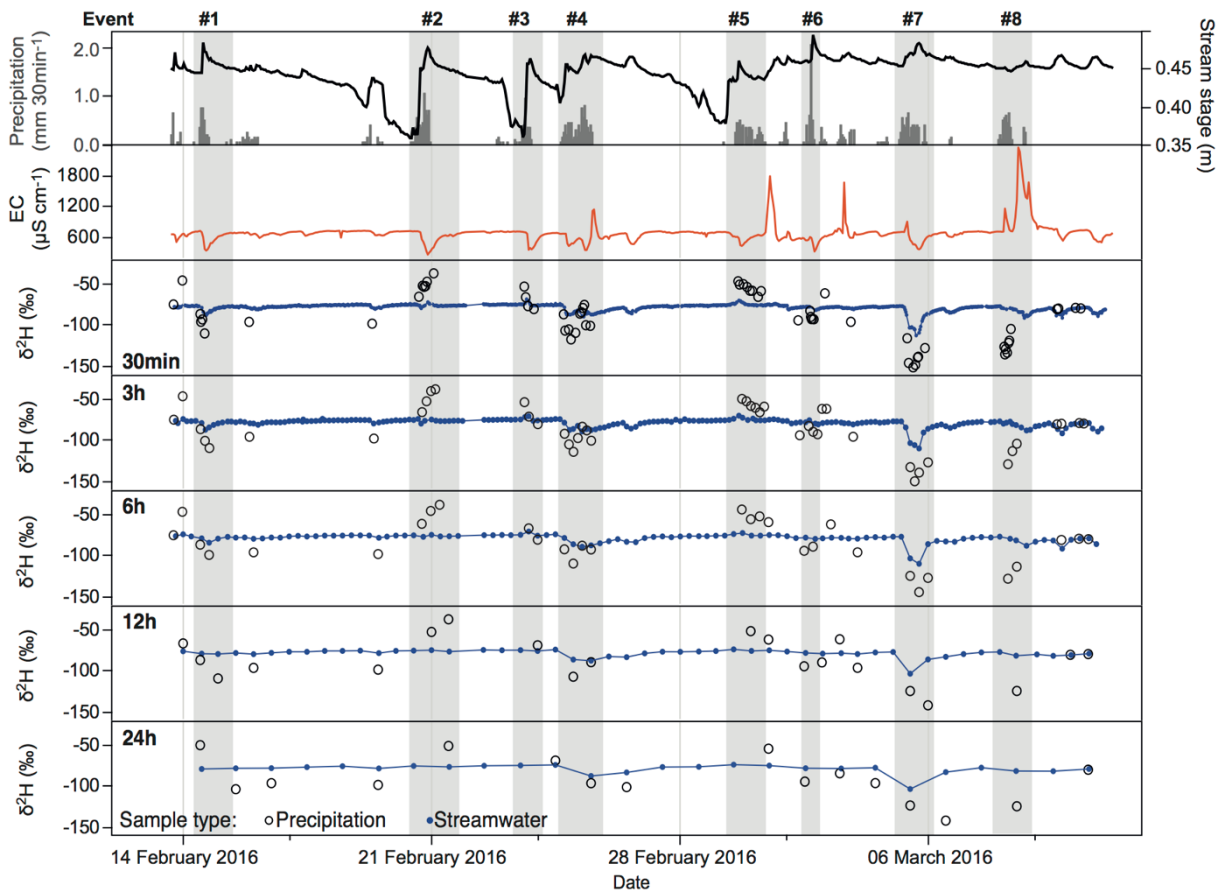
Figure 10: Time series of precipitation, stream stage and streamwater EC, as well as δ²H values in streamwater and precipitation at sampling intervals of 30 min, 3 h, 6 h, 12 h and 24 h. Streamwater isotope values at 3 h – 24 h temporal resolution were obtained by sub-sampling from the 30 min time series. To mimic the effects of integrated bulk precipitation samples, isotope values in precipitation were calculated from volume-weighted averaging the 30 min data over the corresponding time intervals. Vertical grey bars indicate the periods of the eight precipitation events used for hydrograph separation.
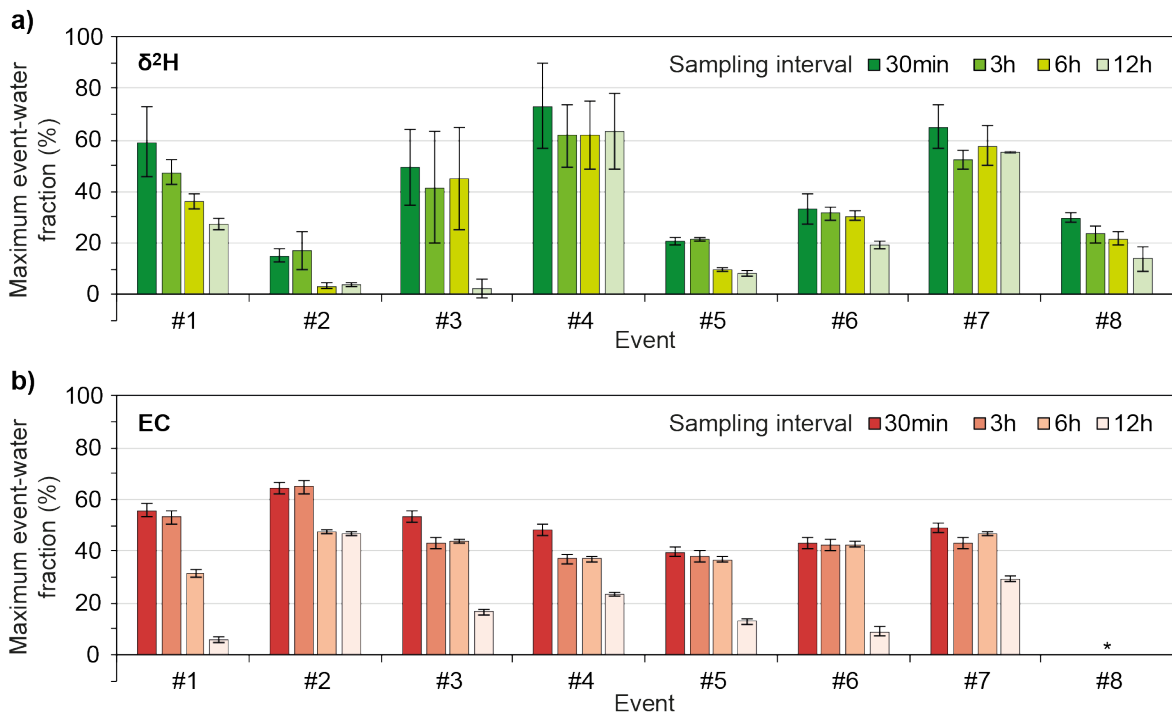
Figure 11: Maximum event-water fractions at sampling intervals of 30 min, 3 h, 6 h and 12 h based on a) δ²H and b) EC. With lower sampling frequencies, the event-water fractions are often underestimated or become even unrealistic, as the likelihood increases that the point of largest δ²H or EC variations in streamflow will be missed (Streamwater δ²H and EC time series were subsampled at 3-hourly, 6-hourly, 12-hourly and daily intervals; concentrations of integrated bulk precipitation samples were calculated from the volume-weighted averages over the respective time interval. For Event #8, wash-off of road salt resulted in unrealistic $F_{E,max}$ values based on EC (*).).